Simplified modelling and pushover analysis of infilled frame structures accounting for strut flexibility

Onur Deniz Akan[1], Gerard J. O'Reilly[1] and Ricardo Monteiro[1]*

[1]Centre for Training and Research on Reduction of Seismic Risk (ROSE Centre), Scuola Universitaria Superiore IUSS di Pavia, Pavia, 27100, Italy

**Corresponding Author,* gerard.oreilly@iusspavia.it

ABSTRACT

Seismic assessment of structures is often performed using their force-displacement capacity or pushover curve computed via nonlinear static analysis. However, these analyses' reliability depends on the numerical model's detail and its ability to capture salient failure mechanisms. Simplified analysis methods offer effective means of identifying structural deficiencies and provide analysts with a sound understanding of key structural characteristics, such as the strength hierarchy, status of the structural damage in terms of limit state exceedance or the progression of the inelastic mechanism, in addition to providing a method with which to check numerical analysis results. This work builds upon the existing literature for simplified analysis of moment frame structures and describes a simplified pushover-based analysis procedure for infilled frame structures. Individual storey responses are obtained by combining the flexural resistance of the frame and accounting for the axial resistance of the infill (modelled as an equivalent axial strut) and the boundary frame members, assuming both systems work in parallel. Then, the displaced shape of the structure is iteratively calculated for a given base shear, which can be repeated until a pushover curve is obtained with relative ease. The proposed procedure is tested and evaluated versus other available methods by analysing several infilled reinforced concrete frames. It is shown that the method can perform simplified pushover analysis with a high degree of fidelity while improving over the other similar methods currently available.

KEYWORDS: pushover; infilled frame; displaced shape; simplified analysis; seismic assessment

1. Introduction

With recent developments in structural analysis and assessment, nonlinear static analysis (NLSA) methods have received increased attention. Among many NLSA methods, static pushover analysis (SPO) is seen as a fast yet robust way of performing seismic analysis (1,2) and is often preferred by engineers as a preliminary step towards more complex investigation, if not chosen as the primary approach. If handled carefully, a straightforward force-displacement curve of a structure, computed through SPO, is a handy tool for the seismic evaluation of existing buildings. Such capacity curves are often used as standard inputs to nonlinear static procedures (NSPs), such as the displacement coefficient method (3), capacity spectrum method (1) or N2 method (2), to name a few. For example, the latter two have been adopted by ATC-40 (4) and Eurocode 8 (5). Furthermore, with the development of simplified tools such as SPO2IDA (6), recently extended by Nafeh *et al.* (7) to infilled reinforced concrete (RC) frames, SPO has been integrated into more advanced approaches like the Pacific Earthquake Engineering Research (PEER) Center's framework (8).

Given the evermore prevalence of irregular structures in earthquake-prone regions, structural engineers may employ detailed analysis techniques such as nonlinear response history analysis (NLRHA), often applied multiple times with several ground motions to cover a wide range of possible scenarios. NLRHA may be considered more attractive than pushover analysis, yet, setting up a sufficiently detailed NLRHA model may be considered a strenuous process due to many crucial decisions, steps required, and variables to control, such as defining suitable modelling methods, element formulations, damping models, material and geometric nonlinearities, integration methods, achieving convergence and selecting suitable ground motion records. Hence, modellers often prefer to start with a simple approach, such as a pushover analysis, in which the number of variables to control is relatively reasonable, and build complexity as it becomes necessary. Currently, a pushover analysis can be done rapidly with various computer programs, such as OpenSees (9), SeismoStruct (10), Ruaumoko (11), or SAP2000 (12). However, like in NLRHA, the reliability of these analyses' results is still determined by the detail and the capability of the model to capture the "true" behaviour of the modelled structure, which may not always be immediately apparent.

Recently, simplified analysis methods have found their place as simple, yet mechanics-based approaches and have been prominently prescribed by most modern building codes worldwide. The main advantage of these simplified methods is that they offer the analyst a good understanding of the structural behaviour by providing direct access to modelling parameters throughout the analysis. Hence, by tracking the progress at each analysis step, the analyst can establish a sound understanding of key aspects of the analysed structure, such as the strength hierarchy, status of local limit states and the progression of the global failure mechanism. In line with the ideology above, an

efficient, simplified pushover analysis procedure for bare frame structures was recently introduced and validated by Sullivan *et al.* (13). The present study builds upon such a methodology, extending it to the analysis of masonry-infilled frames, accounting for their impact in terms of increased frame lateral strength and stiffness due to the strut action introduced by the infill panels.

2. Evolution of simplified nonlinear static analysis

Addressing the need for a structure-specific simplified assessment procedure, Priestley and Calvi (14) introduced a two-step assessment method, later called the force-based method. The structural response is obtained by applying capacity-design principles in reverse and evaluating several capacity indices. Among various novelties proposed by these authors, the sway potential index, S_p, given in Eq. (2.1), was one of the most notable.

$$S_p = \frac{\sum_j (M_{bl} + M_{br})}{\sum_j (M_{ca} + M_{cb})} \quad 2.1$$

In Eq. (2.1), M_{bl} and M_{br} are the expected flexural strengths of the right and left beams connecting to a joint at a given storey, respectively, and M_{ca} and M_{cb} are the expected flexural strengths of the above and below columns. Depending on the value of S_p, it is possible to identify a collapse mechanism, i.e., a column- or a beam-sway mechanism, assuming that a flexure mechanism will govern. Specifically, an S_p lower than 0.85 indicates a beam-sway mechanism, while a column-sway type of failure is associated with a value higher than 1.0.

While emphasising the shortcomings of the so-called force-based methods, Priestley (15) proposed a displacement-based approach for assessing structures, which was later revisited by Priestley *et al.* (16). This procedure's main objective is either to do a pass/fail check of code-compliance or to compute the annual probability of exceedance of one or several limit states using substitute-structure principles introduced by Shibata and Sözen (17). To do so, unlike the previous approaches, the force-displacement response of the structure is computed using a simplified method that considers different equations for empirical displaced shape, yield curvature and yield drift.

Similarly, the ATC-40 (4) proposed a step-by-step, simplified capacity analysis method to compute the pushover curve. The analysis is done applying a first mode based lateral force vector to the structure, solving for the response, updating the state of each member, and repeating the process for an increased lateral force vector. The nonlinear response of the members is modelled by assigning a very low or zero stiffness value once the member fails. Furthermore, an exception is defined for progressively degrading structures, which could be applied to infilled frames. To capture the softening branch of the pushover curve, multiple pushover analyses are carried out in which the analysis is stopped at the peak response, the failed elements removed, and then a subsequent pushover analysis is done until the new peak response. By repeating and joining each peak point, a saw-tooth-like approximation of the degradation response is obtained. However, prior assumptions on the global failure mechanism of the structure and its progression are required.

Even though the aforementioned studies acknowledge the significant effect of masonry infills on the structural response, they do not consider it explicitly. The contribution of the infill panels is either neglected, assuming that they do not interfere with the overall performance or is taken into account as stiffening elements (struts), assuming that the global behaviour stays reasonably unchanged in the elastic range. As shown later in this paper and recognised in numerous experimental test campaigns (18–24) and analytical studies (24–29), these simplifying assumptions made in the past regarding the impact of infill panels do not hold in the majority of cases.

Years later, two coordinated attempts to fill this gap were proposed by Landi *et al.* (30) and Saborío-Romano (31) to consider the effects of the masonry infill panels on the displaced shape of a frame structure. Landi *et al.* (30) suggested obtaining the infilled frame displaced shape by simply scaling those given by Priestley *et al.* (16). On the other hand, Saborío-Romano (31) proposed a different method, in which the drift attained by the infill panels existing at each storey is rendered as additional rotational work done by the infill panel, which is then represented in terms of additional storey moments, hence, causing an increased overall storey stiffness.

Shortly after, another scheme was proposed by Cardone and Flora (32) to incorporate record-to-record variability in the assessment procedure. Similarly to Priestley *et al.* (16), after identifying a likely collapse mechanism, the sway profile of the bare frame is estimated through displaced shape formulas and then scaled based on the anticipated estimate of increased equivalent damping provided by the infills. The effect of stairs is also included by scaling the profile again with empirical reduction factors. These coefficients are iteratively computed by reading off the sub-structure demand from the displacement response spectrum, computing the corresponding equivalent viscous damping value, updating the displaced shape, and repeating until convergence.

Later, the simplified analysis procedure by Priestley *et al.* (16) was revisited by Sullivan *et al.* (13) in an attempt to loosen initial assumptions regarding the displaced shape, given that the existing library of empirical relationships was seen not to be suitable when considering non-ductile frames with masonry infill panels. The

authors proposed a storey stiffness-based iterative method to estimate the displaced shape of the structure for a given base shear, inspired by numerical root-searching algorithms. Hence, the displacements are obtained using the stiffness of each storey instead of using empirical approximations. Notably, however, this approach did not consider the impact of masonry infill panels on the structural response.

More recently, Gentile *et al.* (33) presented the simple lateral mechanism analysis (SLaMA) for the simplified analysis of infilled RC frame structures. In SLaMA, the infill and the frame responses are assumed to be decoupled. The likely failure mechanism is identified for the frame counterpart by conducting strength hierarchy checks at each joint. Based on the outcome, the bare frame response is evaluated either by employing empirical displaced shape functions or step-by-step analysis. In parallel, the infill response, modelled as struts, is computed by considering their axial force capacity. Finally, the two separate curves are aggregated to obtain the combined global response of the structure. Among other minor assumptions that will be described later, a principal limitation of this approach is the neglection of the strut flexibility contribution to the lateral displacement of the infilled frame system.

This paper describes a mechanics-based methodology that accurately estimates the infilled storey stiffness and overcomes the limitations observed by Gentile *et al.* (33) in SLaMA. Then, it presents a simplified analysis procedure that extends the approach of Sullivan *et al.* (13) to sufficiently capture the nonlinear behaviour of an infilled frame system without compromising the ease of implementation.

3. Proposed simplified nonlinear static analysis procedure

3.1. Overview

When calculating the force-displacement curve of a bare frame structure, the idealised output is typically a bilinear curve consisting of an initial elastic part followed by a post-yielding inelastic branch (2,5,13). Such an idealised behaviour would be an oversimplification for an infilled structure since the overall response is nonlinear due to frame-infill interaction, starting well before the global collapse mechanism appears. The reason behind this nonlinearity is the altering global stiffness of the structure as the infill panels begin to damage under relatively low drift ratios (~0.01rads) (19,22,27) compared to frame members, causing multiple stiffness branches to appear, which have been characterised in further detail by Nafeh *et al.* (7), for example. Consequently, a fixed displaced shape function may not be suitable for capturing the deformation state as damage progresses through the various stiffness branches but would require an iteratively computed profile, such as the one proposed by Sullivan *et al.* (13) for bare frame structures. As such, the work by Sullivan *et al.* (13) is taken as a starting point for the procedure proposed in this paper. For simplicity and within an initial formulation of the method, the shear-flexure interaction between the frame members and the effects of shear or joint failure in the boundary beam-column elements are not considered, and only the flexural response of the frame members is investigated. However, the shear capacity of the columns may be computed and checked with empirical capacity models, such as the model by Priestley *et al.* (34), whereas the joints may be checked following similar capacity models (35–38), as part of a post-process to check that shear failure is indeed not an issue. Moreover, only the in-plane contribution of the infill panels, without openings, to the structural response is considered. These aspects may be addressed by using recently published works, including (39–41).

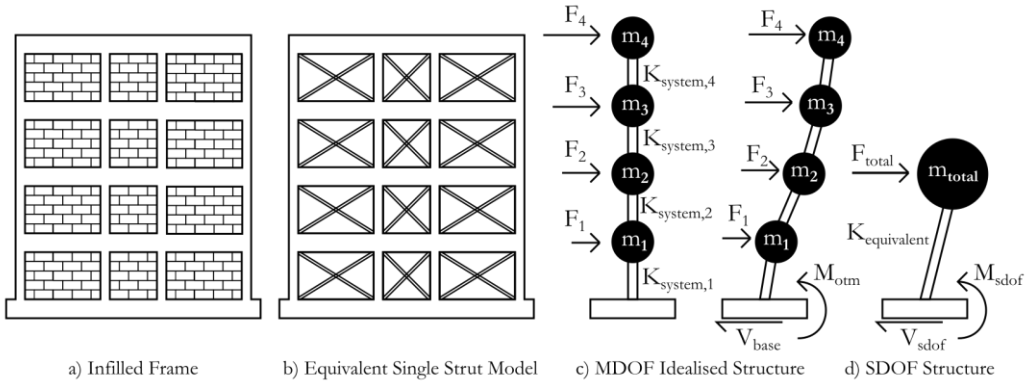

Figure 3.1. (a) Infilled frame structure (b) Single strut model representation (c) MDOF idealised structure representation of the strut model with the estimated storey system stiffnesses, $K_{system,i}$ (d) Final SDOF sub-structure with an applied horizontal force and a resulting displacement

As a first step, the mechanical and geometrical properties of the infilled frame are defined. Infill characteristics are computed using a suitable and widely-used backbone model from the literature (19,42–46) following the single equivalent diagonal strut modelling approach (28,47,48). The infill horizontal force-drift response is computed

for each storey by aggregating all the strut members at that storey. In parallel, the backbone of each frame member is estimated via a moment-curvature analysis. Similarly, for each storey, the lateral frame response is computed by summing the flexural capacity of the frame members. Then, both structural responses are combined to obtain the storey system response of the infilled frame, as shown in Figure 3.1(c), deriving an equivalent multi-degree of freedom (MDOF) stick structure. Next, the MDOF idealised structure is analysed for a given base shear value, and a displaced shape is calculated. Finally, with the acquired displaced shape, the MDOF idealised structure is further reduced to an equivalent single degree of freedom (SDOF) substitute structure (Figure 3.1(d)), which assumes a first mode dominant response, to plot the base shear versus displacement.

For the analysis, the displacement profile of the idealised structure is computed iteratively, as in Sullivan et al. (13). The first mode based lateral force vector is computed by assuming an initial guess displaced shape. Then, the response of the idealised structure is evaluated through storey response functions for a target base shear or a roof displacement. The process is repeated until convergence is achieved. This procedure resembles the first mode-based derivative of the displacement-based adaptive pushover algorithm with an incremental update procedure (49).

3.2. Assessing the lateral resistance of each storey

Estimating the horizontal force-deformation capacity or stiffness of a simple one-bay-one-storey bare frame structure is a routine procedure. Typically, the lateral stiffness of a frame is associated only with the flexural deformation of the frame members, assuming that all the members are axially rigid. While this is a helpful simplification for bare frames, given that the contribution of axial stiffness in the induced horizontal displacement of the frame is minimal, the same simplification cannot be made when masonry infills are present. Infilled frame behaviour is highly dependent on the axial stiffness of the different members of the system, especially in low drift ranges and the flexural stiffness due to the imposed axial deformation introduced by the compression strut formed in the infill panel, as will be shown later.

Crisafulli (24) pointed out that a one-storey-one-bay infilled frame behaves reasonably analogous to a truss system where the load-bearing mechanism is formed through the triangular geometry created by the leading boundary column in tension, the diagonal compression zone of the infill and the infinitely rigid ground. Furthermore, the same truss analogy was shown to be valid also for multi-bay and multi-storey infilled RC structures (24,50). A widespread application of this is the equivalent strut analogy for the numerical modelling of infills, discussed by Crisafulli *et al.* (28), amongst others. Using a strut-type macro-model is a practical way of incorporating the stiffness introduced in the frame system by the infill panel through the definition of an equivalent truss element with an axial stiffness and backbone behaviour. In line with this approach, the present study assumes that the horizontal stiffness of an infilled frame is equivalent to a corresponding composite truss-frame structure.

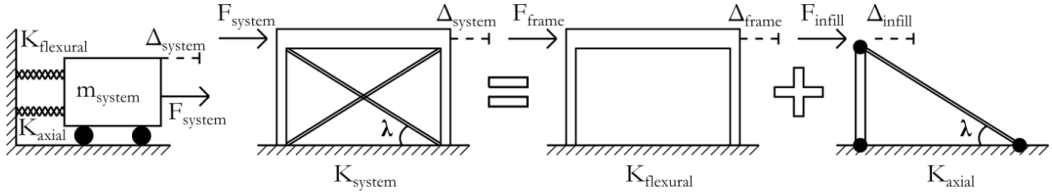

Figure 3.2. (a) Two springs connected in parallel to a mass (b) Superposition of the flexural and the axial stiffness of the system, with the latter comprised of a single diagonal truss and a leading boundary column element

Accordingly, the frame and infill counterparts can be separated into two parallel systems. In this case, the lateral stiffness can be calculated by breaking it down into two sub-structures: a frame (flexural stiffness) and a truss (axial stiffness) system, calculating their stiffnesses and then superposing them with the assumption of two springs connected in parallel to a mass, as illustrated in Figure 3.2(a). The truss system comprises a leading boundary column and a diagonal strut representing the infill panel. As for the parallel spring assumption, the conditions in Eqs. (3.1) to (3.3) are imposed.

$$\Delta_{system} = \Delta_{frame} = \Delta_{infill} \tag{3.1}$$

$$F_{system} = F_{frame} + F_{infill} \tag{3.2}$$

$$K_{system} = K_{flexural} + K_{axial} \tag{3.3}$$

where Δ_{system}, Δ_{frame} and Δ_{infill} correspond to the lateral displacements, F_{system}, $F_{frame,}$ and F_{infill} are the applied external horizontal forces and K_{system}, $K_{flexural,}$ and K_{axial} indicate the horizontal stiffnesses. In the elastic range, for a given $F_{system} = K_{system} \bullet \Delta_{system}$ condition, Eqs. (3.1) to (3.3) have two unknowns (i.e., $K_{flexural}$ and K_{axial}) which are computed through simplified analysis. An external force, F_{system}, is applied, and Δ_{system} is computed. Finally, F_{frame} and F_{infill} are calculated by invoking Hooke's Law. The extension proposed in this work is achieved by estimating K_{axial} introduced by the infills while relying on Sullivan *et al.* (13) to calculate $K_{flexural}$ associated with the frame flexural behaviour, considering the complete response of an infilled frame.

3.2.1. Infill truss system behaviour

The contribution of the infill truss system to the storey lateral stiffness is calculated by first characterising the section-level response, then passing it to the member and storey behaviours consecutively. The output of this approach is a set of individual storey-by-storey infill force-displacement response curves, $F_{infill,(i)} = \beta_i(\theta_{infill,(i)})$, where *i* denotes storey number and β_i is the storey infill response function.

The methodology described in this work is limited to single equivalent diagonal strut models. Future research work may include other modelling strategies, such as double or triple struts, which enable the investigation of the members' potential shear-related response and failure effects. Nevertheless, choosing the most suitable strut modelling methodology for the problem is up to the analyst. Some suggested single strut models include: Bertoldi *et al.* (42), Panagiotakos and Fardis (44), FEMA 356 (3), Decanini *et al.* (43), Crisafulli *et al.* (51), ASCE/SEI 41-17 (52) or Sassun *et al.* (19). Note that, while choosing a model, the model's capability to predict different masonry failure modes is critical. Bose et al. (53) and the references therein discuss the drawbacks of the traditional strut analogy in modelling masonry infills and propose an improved strut model calibrated with experimental or detailed numerical analysis results. Once a suitable modelling approach has been identified, the procedure described next is used to estimate the capacity points and the corresponding stiffness of the infill members.

The section backbone response (strength, stiffness and drift capacity) is obtained for each infill panel using the chosen modelling approach to set up the infill truss system's behaviour. At this point, it is crucial to define the coordinate system utilised for general calculations and the piece-wise linear damage state function that represents the response of an infill panel in a simplified manner.

First, the local member stiffness is denoted by lowercase *k*. In contrast, the horizontal component of the global stiffness is denoted by uppercase *K*. Accordingly, the member stiffnesses are computed in the member's native coordinate system. Meaning the local basis coincides with the natural basis of the member. In contrast, the global stiffnesses are computed in the global coordinate system. Second, the infill's damage state (DS) is defined as a function of axial strut strain, or storey drift, using Eq. (3.4) to keep track of the strut's response state during the analysis. The relationship between the accumulated drift and the damage state for infills has been investigated by various authors, including (19,27). Finally, the limit strain values that defines the interface between consequent DSs are collected in a second function, described by Eq. (3.5), termed the limits function (LF) for ease of representation.

$$DS_{infill}(\theta) = \begin{cases} damage\ state\ 0, & \theta_{infill}^{0} \le \theta < \theta_{infill}^{1} \\ damage\ state\ s, & \theta_{infill}^{s} \le \theta < \theta_{infill}^{s+1} \\ damage\ state\ s+1, & \theta_{infill}^{s+1} \le \theta < \theta_{infill}^{s+2} \\ damage\ state\ N_{DS}, & \theta_{infill}^{N_{DS}} \le \theta < \theta_{infill}^{N_{DS}+1} \end{cases} \quad 3.4$$

$$LF_{infill}(s) = \{\theta_{infill}^{s}, \quad 0 \le s \le (N_{DS}+1)\ where\ s = 0, 1, \dots, (N_{DS}+1)\} \quad 3.5$$

where θ is the storey drift, θ_{infill}^{0} is the storey drift corresponding to initial infill conditions, θ_{infill}^{s} is the consecutive infill drift limit, and N_{DS} is the number of damage states. The LF defines a drift limit which, when exceeded, induces a DS. Therefore, a DS represents a zone of damage between a defined set of N_{DS} number LF limits. The need for such a distinction will become apparent later, but a reference system that is general enough to be used based on storey drift or strut strain and also the current state of the infill panel concerning these limits were deemed necessary. To illustrate this, Figure 3.3 shows a four-limit-valued storey infill response curve obtained by adapting the strut model defined by Sassun *et al.* (19) into the described reference system. The shown process can be applied to any suitable strut backbone conforming to the properties defined earlier in this section.

As the first step, for infill at a given storey, the piece-wise linear strut axial force-displacement response is computed using the tangent strut stiffness k_{strut}^{s}. With the axial stiffness of the infill strut known for any DS, the axial stiffness of the boundary column shown in Figure 3.2(b) is computed. For a typical applied lateral load, the boundary column will be in tension. However, when gravity loading is present on the column, the resultant

behaviour is expected to be initially compressive, followed by some unloading due to the addition of the tensile seismic load. Assuming that the axial column response remains in the elastic range, the boundary column cracked or uncracked axial stiffness in tension can be calculated using the well-known axial stiffness formula. Using the initial stiffness is a reasonable approximation only for a limited initial range where the tensile response is approximately linear (54). For a simplified analysis, the axial behaviour may be assumed to be in this range, hence using uncracked stiffness throughout, whether under compression or tension, ignoring effects like yielding or tension stiffening. However, the axial degradation of the columns can also be taken into account using additional damage states in case it is of interest.

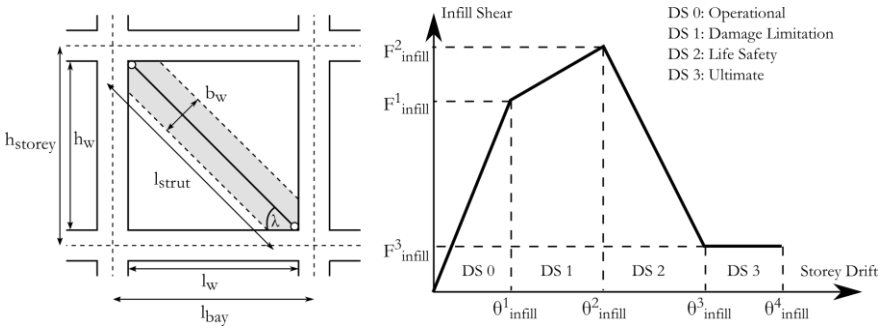

Figure 3.3. A Quadrilinear Infill Storey Response Curve, β_i

The next step is to calculate the storey infill stiffnesses. Following the flexural and axial stiffness decomposition, as in Figure 3.2, the equivalent truss structure representing the axial stiffness of the infilled frame can be treated with any well-known structural analysis procedure. The method of virtual work was chosen for this study since it allows the analyst to write member actions in terms of external forces and structural geometry. The interested reader is referred to Akan (55) for a detailed derivation of the analytical expressions summarised in this section. As illustrated in Figure 3.4, storey infill stiffness is obtained by first calculating the stiffness of a single bay and then summing bay contributions, assuming they are connected in parallel. This simple addition of bays relies on the assumption of axially rigid beams and beams having little or no contribution to the axial stiffness, which past work by Stafford-Smith (50) noted to be a reasonable assumption for infilled frames. Considering the flow of forces through upper to lower storeys, which is a function of the number of bays, geometry of bays and the strut stiffnesses at the below storey, the aforementioned approach is a simplified representation. However, as shown in the case studies presented later in this work, this process yields estimates comparable with those of the numerical analyses.

The bay horizontal axial stiffness is estimated via virtual work by computing the displacement at the top of a single storey due to an applied unitary horizontal force, and then taking the inverse (unit force divided by the displacement, δ). For a single bay ground storey structure (Figure 3.2(b)), the bay infill stiffness calculation is given by Eqs. (3.6) and (3.7):

$$\delta^s_{1j} = \frac{tan^2\lambda_{1j}}{k^s_{column,(1j)}} + \frac{1}{(cos^2\lambda_{1j})(k^s_{strut,(1j)})} \quad 3.6$$

$$K^s_{axial,(1j)} = \frac{1}{\delta^s_{1j}} \quad 3.7$$

where for the first storey, j-th bay, δ^s_{1j} is the expected displacement, λ1j is the infill strut angle and $k^s_{column,(1j)}$ and $k^s_{strut,(1j)}$ are the tangent axial stiffness of the leading boundary column and the infill strut at DS s. Eq. (3.6) is composed of a column term and a strut term: the column term handles the elongation due to the tensile force in the boundary column, whereas the strut term is related to the shortening of the infill strut. The horizontal component of the bay axial stiffness, $K^s_{axial,(1,j)}$, is recomputed at each DS to define the successive branches of the storey backbone.

For multi-storey structures, the axial stiffness of a storey is computed considering the contribution of the storeys below. Since the overturning moment due to the lateral force at a storey is balanced by the moment couple produced by the tension and the compression columns of the storeys below, similar to the rigid storey rotation contribution observed in eccentrically braced frames (56), for example, the resulting additional displacement should be added to calculate the total displacement at a storey. An upper storey is thus expected to be softer than the bottom storey in terms of lateral axial stiffness. The effect of including column axial stiffness becomes significant as the number of storeys increases. This added flexibility of an upper storey becomes apparent in the

structure's overall response, especially if a soft storey is expected at higher levels. The effect of axial stiffness of columns is discussed later in the paper via a case study.

The displacement of a bay is computed again using the virtual work principle, and it results in the expressions given in Eqs. (3.8) and (3.9). The top displacement at the *i*-th storey due to a unit force is computed, including storeys below, as per Eq. (3.8):

$$\delta_{ij}^{s} = \frac{1}{\left(cos^2\lambda_{ij}\right)\left(k_{strut,(ij)}^{s}\right)} + \sum_{a=1}^{i} \frac{tan^2\lambda_{aj}}{k_{column,(aj)}^{s}} + \sum_{a=1}^{i-1} \frac{tan^2\lambda_{aj}}{k_{column,(a(j+1))}^{s}} \quad 3.8$$

$$K_{axial,(i,j)}^{s} = \frac{1}{\delta_{ij}^{s}} \quad 3.9$$

where for the *i*-th storey, *j*-th bay and *s*-th damage state. δ_{ij}^{s} is the expected displacement due to a unit force, and λ_{ij} is the strut angle. As before, the horizontal component of the bay axial stiffness, $K_{axial,(i,j)}^{s}$, can be adjusted by updating (index *s*) the initial column and infill stiffnesses to obtain the successive branches of the storey backbone.

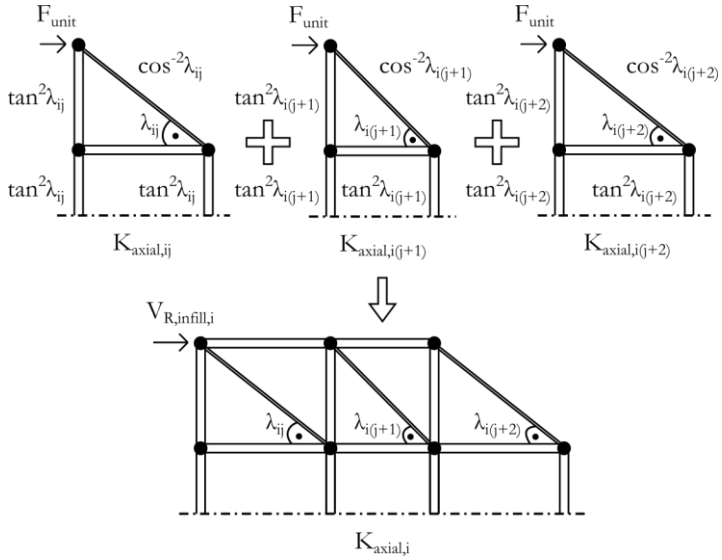

Figure 3.4. Proposed procedure to estimate the storey stiffness by aggregating the consecutive bays and considering the axial shortening and elongation of the lower storeys

For multi-storey, multi-bay frames, such as that shown in Figure 3.4, the total stiffness of the frame can be obtained from Eq. (3.8) by simply adding the individual stiffnesses of the bays, assuming that the top node displacement of each bay is the same. This assumption implies that bays work in parallel to accommodate the applied external loading, giving the generalised solution for the N_{bay} number of bays shown in Eq. (3.10).

$$K_{axial,(i)}^{s} = \sum_{j=1}^{N_{bay}} \left(K_{axial,(ij)}^{s}\right) = \sum_{j=1}^{N_{bay}} \left(\frac{1}{\delta_{ij}^{s}}\right) \quad 3.10$$

Finally, the storey shear resistance due to infills is computed by summing the horizontal components of the infill strut forces, $F_{strut,(i)}^{s+1}$, (i.e. the force in the strut for a given level of displacement) in a storey (Eq. (3.11)).

$$F_{infill,(i)}^{s+1} = \sum_{j=1}^{N_{bay}} f_{strut,(ij)}^{s+1} cos\lambda_{ij} \quad 3.11$$

$f_{strut,(ij)}^{s+1}$ and $\cos\lambda_{ij}$ for the *i*-th storey and *j*-th bay, are the axial capacity of the strut and the strut angle. Finally, the storey drifts corresponding to the computed forces are obtained using the determined storey shear resistance and the initial stiffness, as per Eq. (3.12).

$$\theta_{infill,(i)}^{s+1} = \theta_{infill,(i)}^{s} + \frac{F_{infill,(i)}^{s+1} - F_{infill,(i)}^{s}}{\left(K_{axial,(i)}^{s}\right) h_{storey,(i)}} \quad 3.12$$

where $F_{infill,(i)}^{s+1}$ and $\theta_{infill,(i)}^{s+1}$ correspond to the bounding storey infill shear resistance and storey drift, respectively, whereas $K_{axial,(i)}^{s}$ is infill stiffness for the damage state *s*.

3.2.2. Overview of the frame flexural system behaviour

According to the parallel spring assumption made in Figure 3.2, the approach of Sullivan *et al.* (13) is applied to quantify the bare frame flexural stiffness ($K_{\text{flexural.}}$) and is briefly described here for completeness. The output of this approach is a set of storey-by-storey frame response curves, $F_{frame,(i)} = \psi_i(\theta_{frame,(i)})$ where ψ_i is the storey frame response function. Similar to the infills, the DSs of the frame members are controlled via separate DS and LF functions. Because of this difference, the index p is chosen to control the frame behaviour.

First, the section moment-curvature (M-ϕ) relationships should be computed to define each member's section backbone capacity such as the yield, ultimate and residual moment-curvature values ($M_{column}^{p+1}, \phi_{column}^{p+1}$ and $M_{beam}^{p+1}, \phi_{beam}^{p+1}$). This way, the existing procedure can also be extended to capture the post-peak response of the members. According to Sullivan *et al.* (13), after the computation of the section capacities, the element force-deformation responses are obtained for every single M-ϕ point (starting from yield), and the element responses are condensed into the storey force-drift backbone curve. The maximum joint moment is established, and the maximum possible demand in each member framing into that joint is defined to satisfy the joint equilibrium conditions. With the obtained top and bottom maximum column moments, the storey shear resistance is computed from Eq. (3.13):

$$F_{frame,(i)}^{p+1} = \frac{\sum M_{column,(i)}^{bottom,(p+1)} + \sum M_{column,(i-1)}^{top,(p+1)}}{h_{storey,(i)}} \qquad 3.13$$

where $F_{frame,(i)}^{p+1}$ is the frame storey shear resistance $\sum M_{column,(i)}^{bottom,(p+1)}$ and $\sum M_{column,(i-1)}^{top,(p+1)}$ are the sum of the top and bottom column end moment demands immediately below the joint centrelines. The required member yield drifts are computed through a set of expressions listed in Sullivan *et al.* (13) for different expected mechanisms, such as beam or column-sway, which are assessed using the sway potential index S_p described earlier.

After the critical drift of each relevant (beam or column) member is defined, the storey yield drift is computed by applying the principle of equal external and internal work. Finally, the storey flexural stiffness is computed with Eq. (3.14). Readers are referred to Sullivan *et al.* (13) for further details regarding how pre-yield and post-yield branches of response.

$$K_{flexural,(i)}^{p} = \frac{F_{frame,(i)}^{p+1} - F_{frame,(i)}^{p}}{\left(\theta_{frame,(i)}^{p+1} - \theta_{frame,(i)}^{p}\right) h_{storey,(i)}} \qquad 3.14$$

3.2.3. Assessing the likely mechanism of each storey

Though S_p sufficiently assesses the relative strength of beam and column members at a storey, due to the frame-infill interaction, additional considerations may be required to identify the potential failure mechanism of an infilled frame. As discussed previously, due to the high lateral stiffnesses generally introduced by the infills at a storey, the low drift portion of the structural behaviour is dominated by the infill response. Based on the failure sequence of the infills across the structure or the irregular distribution of infills (e.g. a pilotis frame), significant stiffness differences may occur between two storeys, which can eventually lead to a premature soft-storey type of failure. Understanding this phenomenon is also critical for beam-sway structures hence a method to help identify the potential of a frame-infill interaction driven soft-storey is necessary. In Section 5.2, the altering global mechanism of a bare column-sway frame due to the introduction of a regularly distributed infill is discussed.

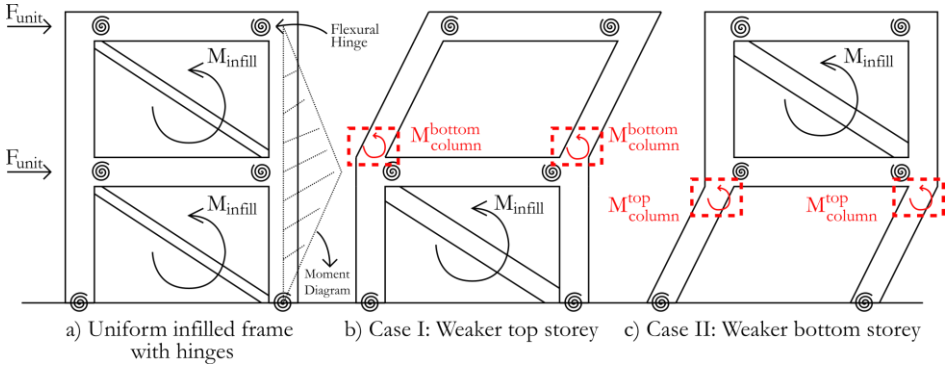

Figure 3.5. The prominent mechanisms for a beam-sway frame designed according to weak beam strong column principles

Consider a beam-sway frame designed according to the weak-beam strong-column capacity design principles displayed in Figure 3.5. Flexural hinges are added at the beam ends and the bottom column end to illustrate the

mechanism forming at the onset of the collapse. Note that without the infill moments (M_{infill}), there is no lateral resistance; thus, the structure is unstable. Case I is achieved if the strength of the infill at the top storey approaches zero and the infill's strength at the bottom storey remains high and vice-versa for Case II. As illustrated, the maximum moments on the columns ($M_{column}^{top} M_{column}^{bottom}$) occurs at the joint level and are equal to the resistance introduced by the infill moments (M_{infill}). Hence, the maximum lateral load applied on the frame can be worked out as the moment that would cause flexural hinging of the top or bottom column sections connecting to the joint.

With a reverse capacity design approach, in which the failure of the columns due to shear is not an issue, if the infill is the weakest link between the column-infill flexural system, the infill would fail before the columns, allowing the stiffer storey to catch up with the softer storey and eventually preserve the beam-sway mechanism. Moreover, in the case of beam-sway structures with uniformly distributed infills (M_{infill} is uniform or similar across the structure's height), pushover analyses show that as the infills at the first floor fail at lower drifts, the structure may transition to Case II following the complete collapse of the infills at the first floor. However, it is important to note that the sharpness of the softening stiffness of the failing infill is an essential factor. For a uniform infilled beam-sway frame, in which the accumulated drift at a storey increases linearly from top storey to the bottom storey, infill failure may happen in a progressive sequence if: (i) the columns can accommodate the internal forces that trigger cross storey infill failure or (ii) the infills at lower storeys exhibit a ductile behaviour.

Assuming that the infills soften with an adequately sharp stiffness and the infill failure occurs at the storey before the drift at the upper storeys catches up, a comparison of column versus infill strengths can be made to identify if a column-sway mechanism is likely. Since a cross storey comparison of the strengths is made, an assumption on the applied lateral force vector is required. Note that a triangular force vector would yield the critical result for Case-I-type of failure, whereas a uniform vector is more critical for Case II. For the sake of simplicity, a uniform force vector is assumed at Eq. (3.15). For a multi-storey, multi-bay, beam-sway infilled frame structure, the potential of having a column-sway failure can be assessed by evaluating the Eq. (3.15):

Pilotis Potential Index, $\boldsymbol{P_p}$ (at joint level)

$$P_{p,i}^{above} = \frac{\sum M_{infill,i}\,(h_{storey,(i+1)})(N-i)}{\sum M_{column,(i+1)}^{bottom}\left(\sum_{a=0}^{N-i}(\sum_{b=i}^{N-a} h_{s,b})\right)} \qquad P_{p,i}^{below} = \frac{\sum M_{infill,(i+1)}\,(h_{storey,i})(N+1-i)}{\sum M_{column,i}^{top}\left(\sum_{a=0}^{N-i}(\sum_{b=i}^{N-a} h_{s,b})\right)} \quad > \mathbf{1.0} \qquad 3.15$$

where $\sum \mathrm{M}_{column,\mathrm{i}}$ denote the elastic column capacity at the *i*-th storey. $\sum \mathrm{M}_{\mathrm{inifll,i}}$ denotes the sum of the peak infill capacity at the *i*-th storey and the infill moments at other storeys at the time of failure of the infills at the i-th storey. $\mathrm{h}_{\mathrm{storey,i}}$ is the storey height, and *N* corresponds to the number of storeys. In the top and the bottom parts of the index equation, the numerator handles the infill-attributed resistance, whereas the denominator is related to the flexural capacity of the columns at the critical section. The double summation term is the overturning moment (OTM) at the storey of interest due to a unit uniform lateral force vector. The maximum storey shear observed before the flexural hinging of the columns is found when the unit OTM is scaled with the capacity of the columns. An outcome greater than one indicates a potential column-sway mechanism at the storey above or below the joint. However, being a purely numerical approach, further research is required to assess the feasibility and accuracy of using Eq. (3.15) in the aforementioned context.

3.2.4. Combining the truss and frame systems

The combined system stiffness merges the estimated horizontal flexural and axial stiffnesses of the frame and the truss system counterparts as per Eq. (3.3) for every storey. The output is, therefore, a set of force-drift curves, $F_{system,(i)} = \zeta_i\left(\theta_{system,(i)}\right)$ for each storey, such as the one illustrated in Figure 3.6, where ζ_i is the storey response function. As before, since the DS and LF of the system are new ones (superposition of infill and frame), the index *k* is chosen to control storey behaviour.

Recalling the parallel springs assumption on the superposition of the flexural and axial stiffnesses in Figure 3.2(b), since both infill and frame counterparts attain the same top displacement, the abscissa of function ζ_i consists of the drift limits of both infill (β_i) and frame (ψ_i) storey behaviour functions in sequentially ascending order, conforming to the strength hierarchy of the storey. Similarly, in between consecutive drift points, the system storey stiffness is given by a direct summation of infill and frame stiffnesses for a given storey level, as per Eq. (3.16). Finally, the corresponding storey shear is computed for the fixed stiffness and drift values, as in Eq. (3.17):

$$K_{system,(i)}^{k} = K_{flexural,(i)}^{p} + K_{axial,(i)}^{s} \qquad 3.16$$

$$F_{system,(i)}^{k+1} = F_{sysytem,(i)}^{k} + K_{system,(i)}^{k}.\left(\theta_{system,(i)}^{k+1} - \theta_{system,(i)}^{k}\right).h_{storey,(i)} \qquad 3.17$$

where $K^{k+1}_{system,(i)}$, $K^{p+1}_{flexural,(i)}$ and $K^{s+1}_{axial,(i)}$ are the system, flexural and axial stiffnesses for the *i*-th storey and damage state *k*, while $F^{k}_{sysytem,(i)}$ and $F^{k+1}_{sysytem,(i)}$ are the storey shears at level *i*.

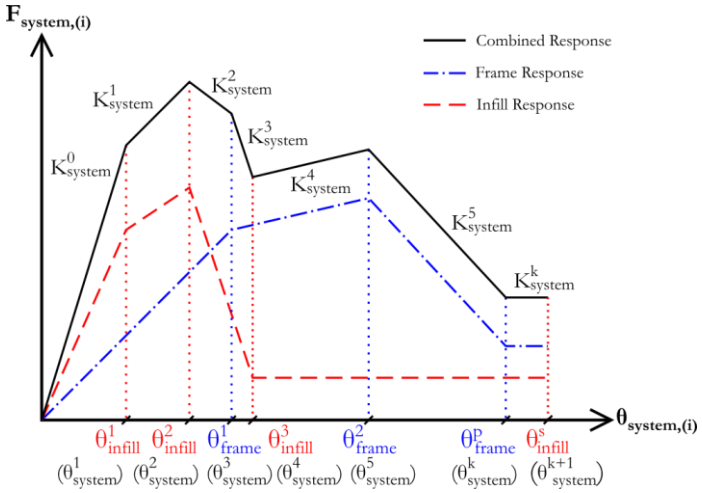

Figure 3.6. Storey response curve $\boldsymbol{\zeta_i}$ for the *i*-th storey. Note that the resultant response is the superposition of individual frame and infill behaviour.

4. Method of analysis

4.1. Summary of the proposed procedure

Following the different steps outlined in the previous section, the analysis procedure to compute the entire force-displacement response of the structure is described here, according to the flowchart in Figure 4.1**Error! Reference source not found.**. By preparing the simplified structural model with sufficient accuracy, following Section 3.2, the structure is condensed into a simplified MDOF structure, where each storey is associated with a horizontal translational degree of freedom. The equivalent structure is analysed following a set of basic steps, similar to those described in Sullivan *et al.* (13) for bare frames, integrated with several extensions to include frame-infill interaction and improve the pre-and post-yield stages of the structural response.

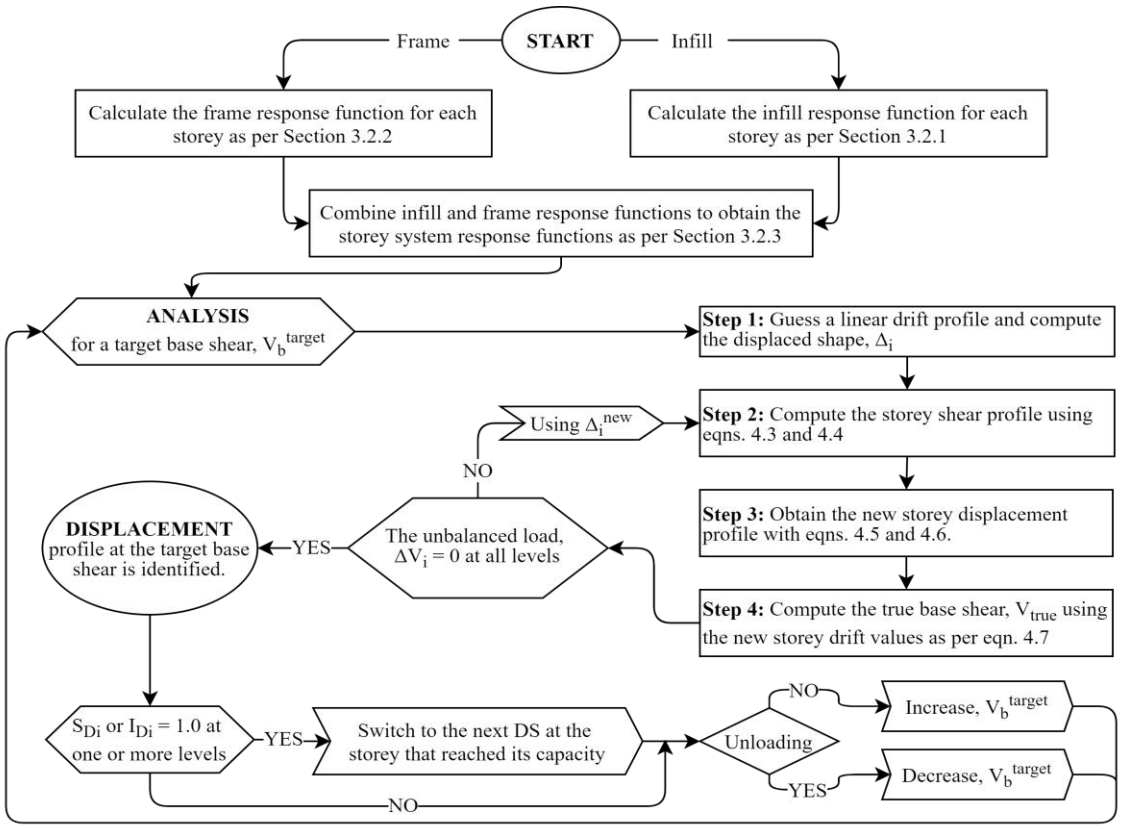

Figure 4.1. Flowchart of the proposed simplified analysis procedure for infilled frames

First, a target base shear is chosen, corresponding to the demand for which the displaced shape will be computed. Next, a storey drift profile is trialled for the structure, and the displaced shape is computed. The external storey shears are computed using Eqs. (4.3) and (4.4). Then, a new displaced shape is obtained applying Eqs. (4.5) and (4.6). For the new displaced shape, the internal (element) forces are computed (Eq. 4.7), and the unbalanced load at each storey is checked (Eq. 4.8). If the convergence is not yet achieved, another iteration is made by repeating Eqs. (4.3) to (4.8) using the new displaced shape. Convergence is achieved usually after three or four iterations, as also noted by Sullivan *et al.* (13). At this point, a capacity point on the pushover curve of the structure is identified, as well as other local engineering demand parameters that may be of interest.

The demand indices S_{Di} and I_{Di} are checked before changing the target base shear and moving on to the next point. These indices provide information regarding the remaining capacity of the frame and infill members. If the capacity is reached at one or more demand indices, it is necessary to alter the storey response by switching to the following damage state's stiffness, drift, and resistance parameters. The complete pushover curve of the structure is obtained by repeating this process, as will be illustrated in Section 5.

4.2. Behaviour indices

Some aspects of the proposed procedure are worth discussing further. If a mechanism due to a possible shear failure in the columns, beams and joints is excluded, the global mechanism of the structure is dictated by the flexural capacity of the frame members, making the sway potential index, S_{p}, compatible with the method discussed in this work to identify the likely storey mechanisms. As an additional step, the potential of having a column-sway type of failure or a beam-sway mechanism due to the frame-infill interaction is assessed by the pilotis potential index, P_p at each joint level (Section 3.2.3).

As the infill and the frame contributions are assumed to be parallel, the frame and infill capacities can be assessed separately. Hence, the sway demand index, S_{Di}, proposed by Sullivan and Calvi (57), can be used to check the capacity ratio of the frame system. It is computed as per Eq. (4.1):

$$S_{Di} = \frac{storey\ i\ frame\ shear\ demand}{storey\ i\ frame\ shear\ resistance} = \frac{F^{t}_{frame,(i)}}{F^{p+1}_{frame,(i)}} \tag{4.1}$$

where index *t* controls the iteration step. Similarly, a check is also done for the infill truss system. The infill demand index, I_{Di}, presented in Eq. (4.2), is computed to check the capacity ratio of the infill panel members of the parallel infill truss system during the analysis.

$$I_{Di} = \frac{storey\ i\ infill\ shear\ demand}{storey\ i\ infill\ shear\ resistance} = \frac{F^{t}_{infill,(i)}}{F^{s+1}_{infill,(i)}} \tag{4.2}$$

$F^{t}_{frame,(i)}$ and $F^{t}_{infill,(i)}$ are computed using Eq. (4.7). Sway and infill demand indices are used in parallel to follow the current response of each frame and infill member in the structure during the simplified pushover. As these indices reach 1.0, indicating that the capacity has been reached, the corresponding member's properties should be updated to the next branch of its backbone curve. Indices possess a crucial role in identifying the structure's degradation pattern and progressive collapse mechanism.

4.3. Convergence and iteration for the displaced shape

The displaced shape, similar to Sullivan *et al.* (13), is iterated over Eqs. (4.3) to (4.6) until a two-step convergence criterion is satisfied. As a start, a trial drift profile is assumed for the structure and, based on the storey displacements, the target base shear is distributed to each storey (Eq. (4.3)). Then, the storey shear profile is computed (Eq. (4.4)), and the storey displacements are obtained by dividing the storey shear by the storey stiffness (Eq. (4.5)). Finally, the new displaced shape is computed (Eq. (4.6)). The first convergence criterion is achieved when the computed displacements (Δ_i^t and Δ_i^{t+1}) are close to each other with an acceptable margin of error (<1‰).

$$F_i^t = \frac{m_i \Delta_i^t}{\sum m_i \Delta_i^t} V_b^{target} \tag{4.3}$$

$$V_i^t = \sum_{j=i}^{N_{storey}} F_j^t \tag{4.4}$$

$$[loading] \qquad \delta_i^t = \frac{V_i^t - F_{system,(i)}^k}{K_{system,(i)}^{k+1}} + \theta_{system,(i)}^k . h_{storey} \tag{4.5.a}$$

$$[unloading] \qquad \delta_i^t = \frac{V_i^t - F_i^{unloading}}{K_{system,(i)}^{unloading}} + \theta_i^{unloading} . h_{storey} \tag{4.5.b}$$

$$\Delta_i^{t+1} = \sum_{j=i}^{N_{storey}} \delta_j^t \tag{4.6}$$

where indices *t*, *i* and *k* control the iteration step, the storey number, and the DS of the storey, respectively. Variables m_i, F_i^t and V_i^t correspond to the storey mass, shear, and cumulative storey shear. If the storey is unloading, $F_i^{unloading}$ and $\theta_i^{unloading}$ are the last computed storey shear and drift values for that storey before the unloading starts, as discussed in the next section. Finally, the target base shear V_b^{target} is the point to be computed on the pushover curve. $F_{\text{frame,i}}$ and $F_{\text{infill,i}}$ are computed based on the computed displaced shape, Δ_i^{t+1} by passing the corresponding storey drift to the infill (β_i) and the frame (ψ_i) storey response functions defined in Sections 3.2.1 and 3.2.2. The storey shear resistance is computed by adding the individual contributions (Eq. 4.7).

$$V_{true,i}^t = F_{frame,(i)}^t + F_{infill,(i)}^t$$
$$where\ F_{frame,(i)}^t = \psi_i(\theta_i^t), F_{infill,(i)}^t = \beta_i(\theta_i^t), and\ \theta_i^t = \delta_i^t / h_{storey} \tag{4.7}$$

Hence, the storey unbalanced load, ΔV_i, can be used as a second convergence criterion (Eq. 4.8). The unbalanced load is computed as the difference between the storey shear (Eq. 4.4) and the true storey shear (Eq. 4.7). The second condition of convergence is reached when the unbalanced load approaches zero. In a continuous analysis, the trialled displaced shape can be taken as the displacement profile obtained from the latest committed step to achieve convergence faster.

$$\Delta V_i^t = V_{true,i}^t - V_i^t \tag{4.8}$$

4.4. Unloading

The final aspect to consider is the localisation of the displacements at the soft-storey. As the analysis progress, infills at one or more storeys may reach their peak capacity. According to the strut backbone, following the peak response, the stiffness of the infill members become negative, indicating a progressively degrading behaviour. At the global level, the applied horizontal load reaches a maximum and needs to be decreased from this point onwards to achieve convergence. Hence, the degrading storeys keep deforming, while the others unload as the analysis progresses. This behaviour causes the source of displacement increment to localise at the soft-storey.

In a simplified analysis framework, the localisation phenomenon is modelled by updating the response of the structural members. When the stiffness of one of the storeys become negative, Eq. (4.5a) is again used to compute new inter-storey displacement values, whereas the remaining storeys proceed with the unloading sequence, switching to Eq. (4.5b). The storey unloading stiffness is a modelling decision and can be explicitly chosen by the analyst for each problem or as suggested by the backbone strategy. The effect of the member unloading stiffness on the global behaviour is partly represented by the slope of the dropping portion in the pushover curve (58), as illustrated in Figure 4.2. By considering the effect of the changing strength characteristics of each storey as the analysis progresses, a global failure mechanism is identified without making any prior assumptions.

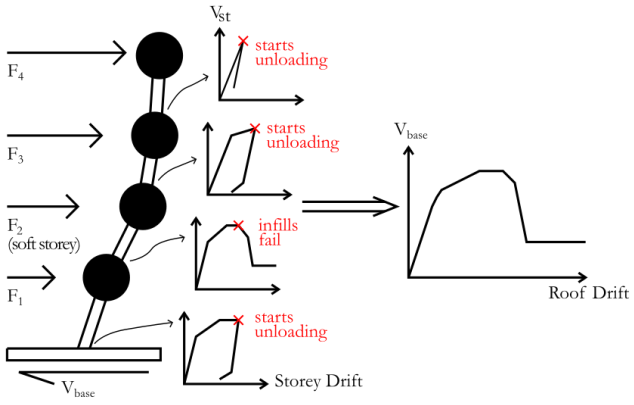

Figure 4.2. The unloading phenomenon and the localisation of deformation at the soft-storey.

5. Validation of the proposed simplified analysis procedure

5.1. Case study structures

A set of existing infilled frames was analysed in OpenSees (9) and with the proposed method (Figure 4.1**Error! Reference source not found.**) to compare the resulting pushover curves. These frames were adopted from the work of Galli (59), who studied the behaviour of multiple frames designed between the 1950s and 1970s, considering them as a sample of the gravity load designed frames in Italy and the Mediterranean region in general. These frames have also been employed in other studies (7,13,25,26,60). For this study, twelve planar frames featuring two different heights, two different widths and three different infill typologies were considered (Figure 5.1). The definition of different typologies of infills was adapted from Hak et al. (27). As modelling decisions, the frame section flexural response was modelled using the approach proposed by O'Reilly and Sullivan (38) for non-ductile RC frame structures in Italy. That study (38) recommended a trilinear backbone curve for the frame members with four performance points. Meanwhile, the infill strut axial backbone was modelled after Sassun et al. (19), in which the backbone presented by Decanini et al. (43) was calibrated with experimental results. The chosen strut model considers compression at the centre of the panel, compression of corners, sliding shear failure, and diagonal tension as possible masonry failure modes. The backbone curve obtained was a quadrilinear curve and consisted of four limit state definitions. The unloading stiffnesses are assumed to be the same as initial stiffness for the sake of simplicity.

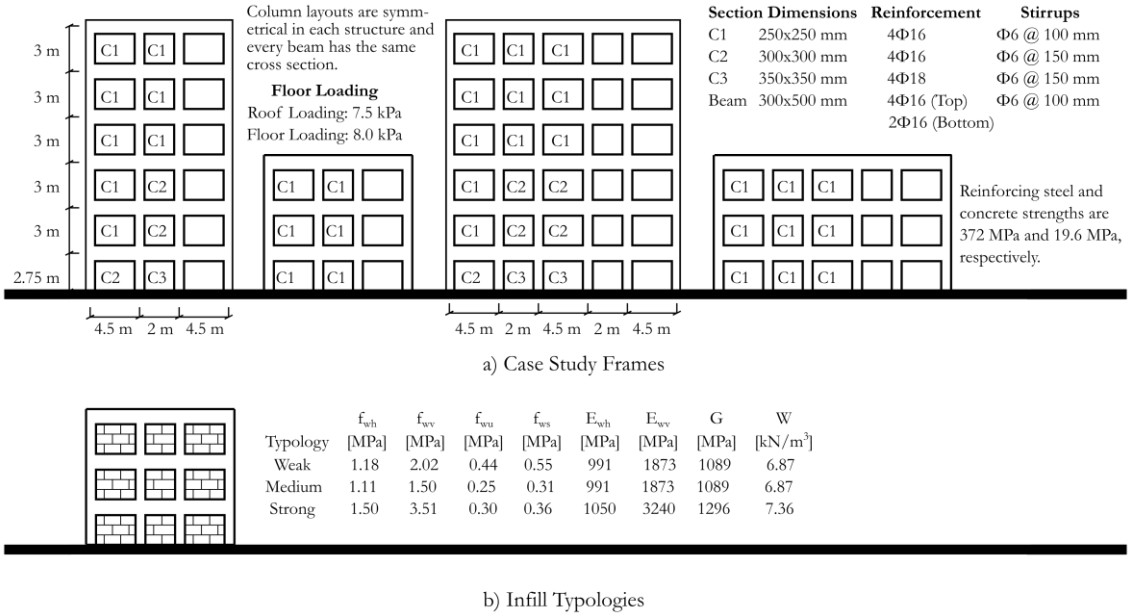

Figure 5.1. (a) The set of 2D frame structures adopted from Galli (59) (b) Illustration of the infill typologies and the uniform distribution adopted

For the simplified analysis, a moment-curvature analysis for the member cross-sections was carried out following the strategy in (38) to identify the yield strength of the members, and the infill strut backbones were evaluated. Calculations were performed in Microsoft Excel, corroborating the practical nature of the procedure, and the spreadsheet of each structure is available on GitHub at: https://github.com/odakan/Simplified-Pushover-Analysis-of-Infilled-Frame-Structures. In OpenSees, beams and columns were modelled using the force-based beam with hinges element. The internal region of the beam-column element was modelled as an elastic section. The endpoint integration method was used at the hinges in which the curvature at the beam end was assumed to be constant over the whole plastic hinge region (61). At each extreme Gauss point, a section aggregator was employed in which a calibrated Pinching4 material provided the flexural section response, as per O'Reilly and Sullivan (38), and the axial response was modelled as elastic. Infills were modelled as single diagonal struts using the truss element. The axial backbone recommended by Sassun et al. (19) was modelled with the Pinching4 material.

5.2. Lateral force-displacement response

SPO analyses with triangular horizontal force vector were carried out on the case study structures in OpenSees, and five displaced shapes, corresponding to different roof target displacements along the pushover curve of each structure, were evaluated. These points were identified by studying the pushover curve to represent the altering

global stiffness and the characteristics of the analysed structure. The comparison between the proposed and the numerically computed pushover curves, displaced shape profiles and the lateral force profile obtained can be seen, for some of the frames, in Figure 5.2 to Figure 5.5 below.

In Figure 5.2, compared with the OpenSees model, the proposed method accurately captures each structure's initial stiffness and peak resistance. The post-peak drop in capacity upon infill failure is reasonably captured by the method as well. In addition, observing the progression of the displaced shapes, the ability of the proposed method to identify the inelastic mechanism is noteworthy. Both analyses indicate failure due to a soft-storey development at the second storey for the six-storey frame and the first floor for the three-storey structure (Figure 5.3 and Figure 5.4). For the 3-bay bare frame versions of these frames, Sullivan *et al.* (13) identified soft-storey mechanisms at the fourth and the second storeys instead, respectively. This discrepancy indicates that the proposed method can capture the frame-infill interaction induced effects in the global mechanism of the infilled frame.

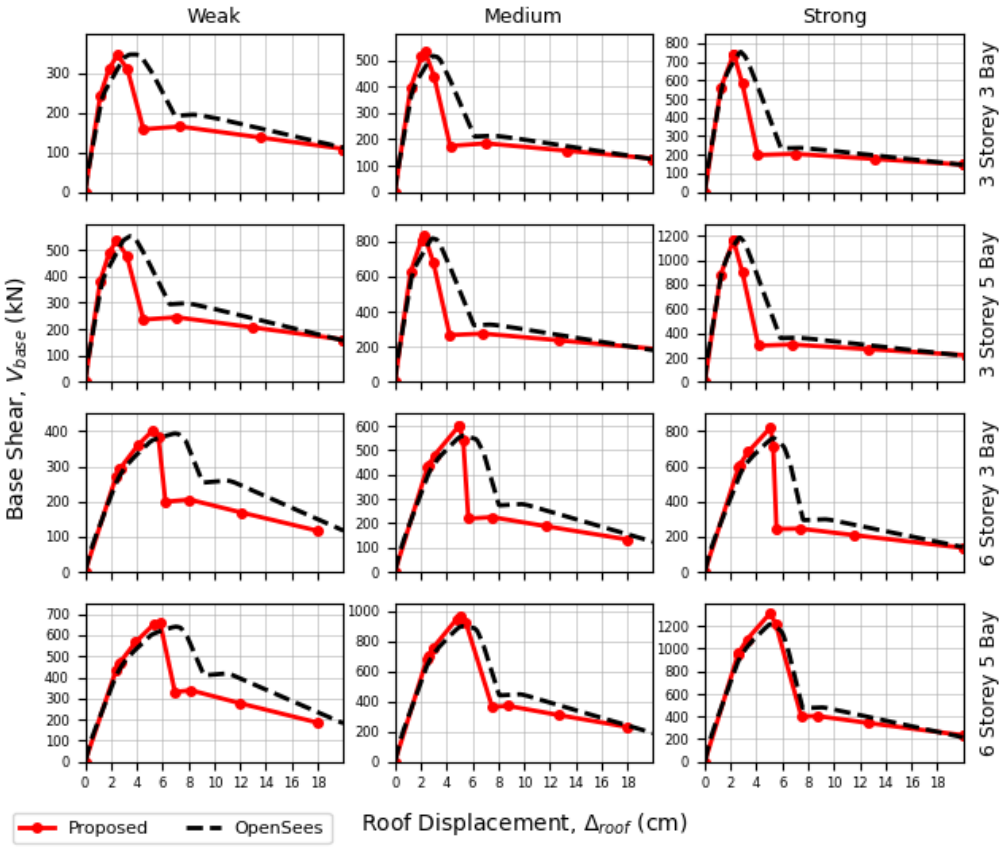

Figure 5.2. Proposed versus OpenSees obtained pushover curves of all twelve infilled frame structures

In Figure 5.4, a roof displacement of 4cm results in cracking the infill panels at the second, first, third and fourth storeys, in the given order. The soft-storey develops approaching the 6cm mark at the second floor, as indicated by the infill demand index. At this stage, the infill panels at the second storey have a negative stiffness, and the other storeys are unloading, as described in Section 4.4. Hence, the drift demand at the second storey dramatically increases, transferring the lateral shear carried by the infills to the surrounding frame. Eventually, since the strength of frame members at the soft-storey is capable of carrying the demand at an inelastic hardening state, the structure transforms into the aforementioned Case II (Figure 3.5), where a potential weak storey is expected at the second storey even though the identified mechanism is a beam-sway at this level using only the sway potential index. Finally, at 8cm roof displacement, a column-sway mechanism forms at the second storey following the flexural hinging at the top and bottom sections of the columns. The pilotis potential index computed at the first and second joint levels indeed yields a value higher than one, indicating an expected column-sway mechanism at the second storey, which aligns well with the logic discussed in previous sections.

In Figure 5.3 and Figure 5.4, it is worth noting that the proposed method effectively captures the overall and local softening of the structure as the infill panels yield and eventually fail. There is an excellent match between the displaced shapes obtained through pushover and the simplified method concerning the first two and last displacements analysed (i.e., 2cm, 3cm, and 10cm). Regarding the other two points examined (i.e., 6cm and 8cm), the discrepancy between the profiles follows a consistent pattern in every case study structure. The discrepancy

between the observed deformation capacities is attributed to the OpenSees model's ability to capture the redistribution of forces between bays and the transition between global mechanisms due to frame-infill interaction. Nevertheless, the overall matching and identification of the mechanism location are deemed satisfactory.

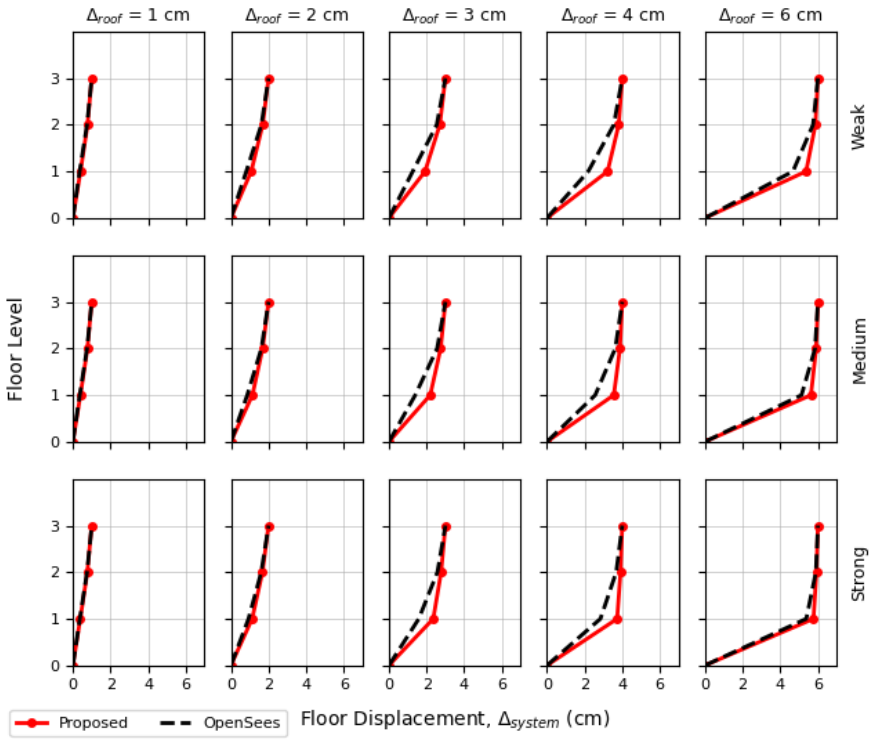

Figure 5.3. Proposed versus OpenSees obtained displaced shape profiles for the 3-storey-3-bay infilled frame

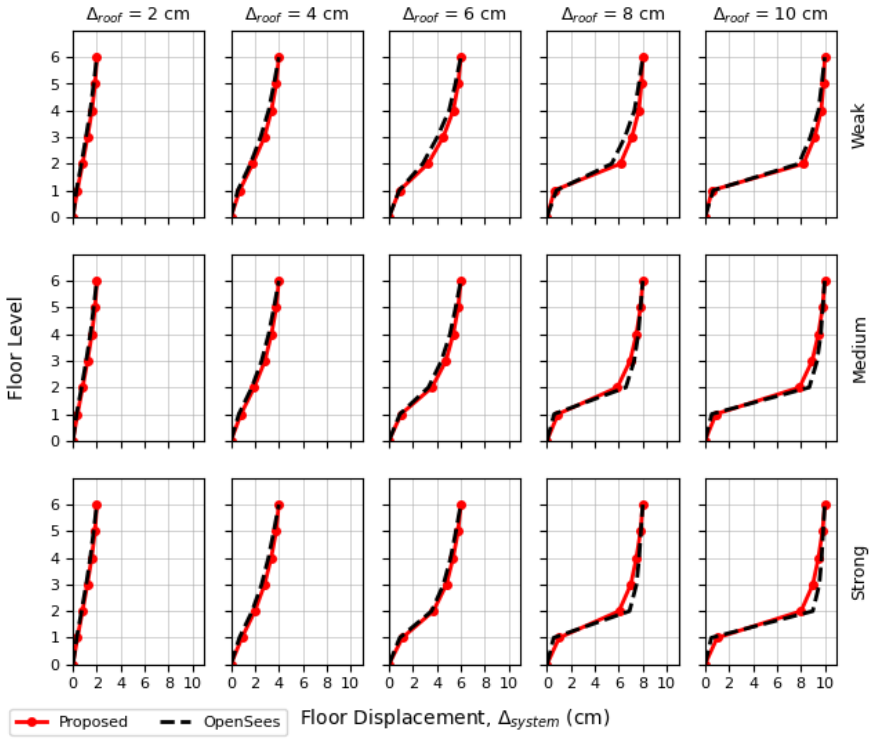

Figure 5.4. Proposed versus OpenSees obtained displaced shape profiles for the 6-storey-5-bay infilled frame

Finally, in Figure 5.5, the evolution of the computed force vector based on the changing first mode shape of the structure at each step can be observed. At the first displacement level examined (i.e., 2cm), except for the last floor, the force vector can be seen to increase linearly with height. Once the structure softens, the force vector gradually becomes more non-uniform as it adapts to the change in the stiffness distribution across the structure's

height. This progression is akin to the adaptive pushover methods available in the literature (49), whereby the load pattern adapts and responds to the structure's altering stiffness distribution and mode shape.

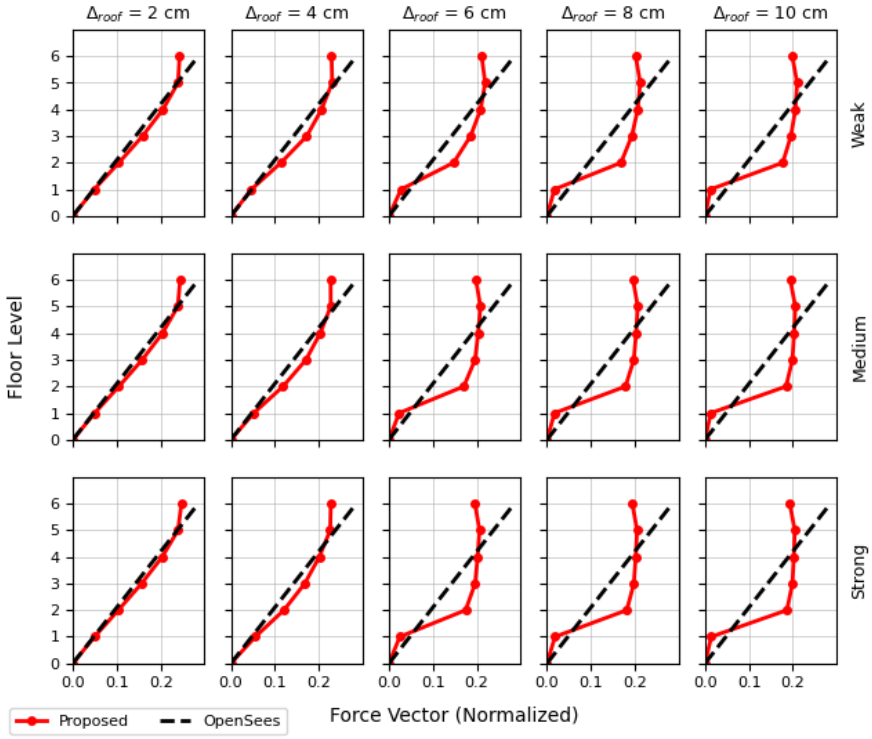

Figure 5.5. Proposed versus OpenSees applied horizontal force profiles for the 6-storey-3-bay infilled frame

5.3. Comparison with other available approaches

First, the method proposed by Saborío-Romano (31), in close collaboration with Sullivan *et al.* (13), was evaluated. According to this methodology, the drift attained by the infill panels was rendered as the additional rotational work done by the storey moments and a stiffness value associated with the total work done by the infill panels at a storey is computed. No consideration is given to the effects of the axial flexibilities at the lower storeys. Finally, the displaced shape is computed using the secant stiffness as the characteristics of the structure updates. Since there are no considerations on the unloading behaviour of the frame, it was only possible to compute the structure's response until the peak capacity.

Second, Gentile *et al.* (33) presented a simplified framework (SLaMA), an alternative to the procedure presented by Sullivan *et al.* (13), in which only the strut stiffness is utilised to estimate the infill contribution of the storey stiffness. For column-sway structures, SLaMA recommends a step-by-step procedure in which the displaced shape of the structure is computed using the secant stiffness corresponding to the updated state of the structure. The infill and frame responses are computed separately and then superimposed to obtain the infilled frame response. The soft-storey is identified as the storey having the lowest strength. Finally, the analysis is done by introducing drift at the soft-storey and calculating structural response.

In light of the present study's findings, some remarks to the procedure described by Gentile *et al.* (33) are presented. Since the failure mechanism considered for the bare frame structure may be altered due to frame-infill interaction, identifying a specific mechanism for the infilled structure could be handled more accurately. First, the authors suggest that the procedure described by Gentile *et al.* (33) to identify the soft-storey for bare frames should be repeated considering the cumulative (peak infill + frame) resistance at a storey. Second, the pilotis potential index at each storey (Eq. 3.15) can be evaluated to ensure that a column-sway type of failure is avoided for a beam-sway frame, as described in Section 3.2.3. Subsequently, the use of secant stiffness makes the evaluation of the post-peak response impractical since the effect of unloading and localisation cannot be considered, as discussed in Section 4.4. This simplification results in unrealistic displaced shapes after the peak response, missing the permanent deformations accumulated at the soft-storey following a reduction in the base shear. Hence, two different approaches were adopted to compute the softening part of SLaMA for the comparison presented here. Based on the interpretation of the illustrations in Gentile *et al.* (33), SLaMA A assumes that the infills at the soft-storey continue to soften until the frame at the same storey fails. This assumption enables the use of the storey secant stiffness after the peak by assuming a hybrid softening stiffness. On the other hand, SLaMA B uses the

secant stiffness for the soft-storey and assumes an infinite unloading stiffness. An infinite unloading stiffness indicates that the unloading storeys will keep their attained drifts as the storey shears decrease due to unloading. Both versions of SLaMA analysed here align with the presented method and merely reflect how one analyst may interpret and implement it versus another.

Finally, Proposed A considers the added flexibility due to the columns' axial stiffness, which is one of the critical developments of the proposed approach not considered in other methods in the literature. In contrast, Proposed B considers the columns as axially rigid. The force-displacement curves and the associated displaced shapes computed using these different methodologies are given in Figure 5.6 and Figure 5.7.

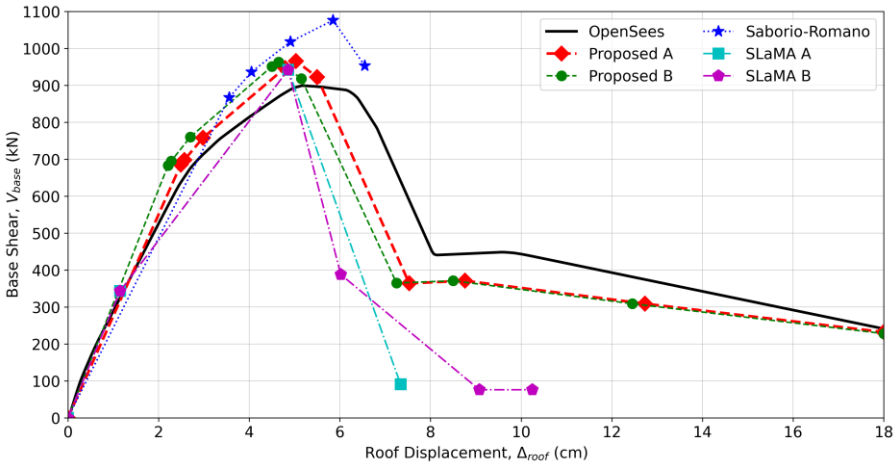

Figure 5.6. Comparison of the force-displacement behaviour obtained with existing approaches for the 6-storey 5-bay medium infilled frame

In Figure 5.6, the initial stiffness is captured by all methods satisfactorily. Compared to the others, Proposed B overestimates the initial stiffness since it ignores the strut flexibility of the columns. This aspect gets notably improved with Proposed A compared to the OpenSees model result since the axial flexibility of the columns is captured in the OpenSees model. Both SLaMA interpretations seem to underestimate the stiffness, while Saborio-Romano gives the best estimate with a slight underestimation. The main reason for this discrepancy is that SLaMA and Saborio-Romano approaches rely on the secant stiffness, whereas the proposed method is based on tangent stiffness. SLaMA and the proposed method yield similar values at the peak response, while Saborio-Romano overestimates the response mainly due to the smearing of the infill strength between the consecutive storeys. Moreover, as an advantage of employing the tangent stiffness, besides capturing the critical aspects of the structure, the proposed method can trace the intermediate characteristics as well such as the progressive cracking of the infill panels across storeys, unloading, failure of the infill, reloading of the frame and the final softening of the structure. Similar to the step-by-set method in ATC-40, in the proposed method, the structural response is computed incrementally, and a zero stiffness is assigned for the fully damaged elements, following the prescription of the chosen backbone model. However, the proposed method can capture the progressive degradation of the structure in a single attempt without computing multiple pushover analyses, yielding a continuous curve, and does not require prior knowledge about the global mechanism.

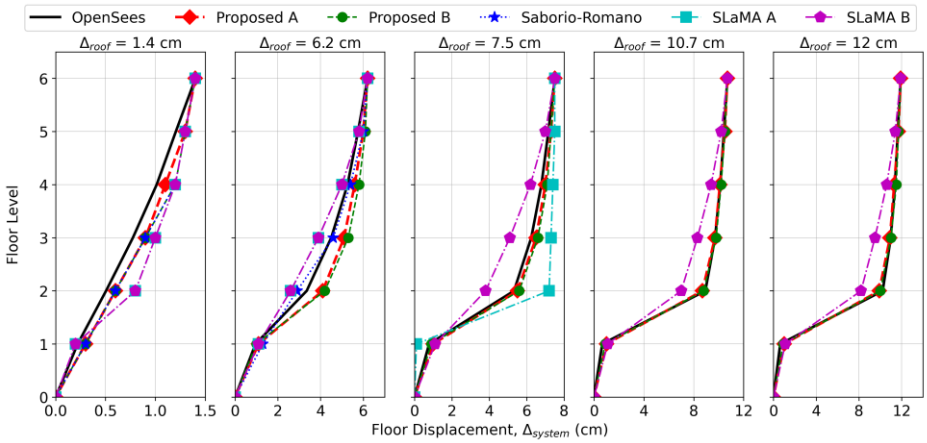

Figure 5.7. Comparison of the sway profiles obtained via existing methods for the 6-storey 5-bay medium infilled frame

In terms of the displaced shapes (Figure 5.7), the method by Saborío Romano (31) cannot capture the existing irregularity in height (stiffer first storey), given that the contribution of the consecutive storeys is averaged. In the case of SLaMA, the characteristics of the infilled frame are more pronounced. The effect of using secant stiffness after the peak can be seen at a displacement of 7.5cm. In SLaMA A, the floors except the soft storey reset when the base shear is reduced. SLaMA B is an improvement, but due to the infinite unloading stiffness, high permanent displacements at the unloading storeys result in a deviated response.

6. Summary and conclusions

A simplified static analysis method was presented to allow analysts to estimate the force-displacement response of an infilled RC frame without resorting to sophisticated analysis tools. The proposed method was built upon an existing framework for the simplified analysis of bare frames susceptible to non-ductile mechanisms, typical of older buildings, built before the emergence of modern design codes. The novelty of the proposed methodology refers mainly to the capability of estimating the storey stiffness considering the contribution of the infill panels and frame-infill interaction. Furthermore, it includes several refinements to the iterative analysis procedure that extend the existing framework to capture the highly nonlinear behaviour of the infilled frames. First, the horizontal flexural stiffness of the bare frame and axial stiffness of the infills were computed by assuming that both systems work in parallel against the external forcing action. Then frame and infill counterparts were superposed to obtain the combined storey tangent stiffness. A novel index was proposed to make additional considerations on the global mechanism of an infilled frame and in the case of a beam-sway frame to check if a column-sway failure is possible. Implementation wise, an unbalanced convergence criterion was introduced, and the infill demand index, I_{Di}, was proposed. Finally, the effects of drift localisation were incorporated into the analysis.

As per Figure 3.4, bays are assumed to work in parallel. Due to this assumption, the complicated flow of forces from upper-storeys to the supports is significantly simplified. As a result of superposing the frame and the infill response, changes in the frame and infill capacity due to frame infill interaction are ignored, as explored further by Bose et al. (53). Pilotis Potential Index (Eq. 3.15) assumes infills do not carry any shear loading after peak response. Furthermore, a uniform horizontal load vector is assumed across the structure's height for the sake of simplicity. The response of the infilled frame is assumed to be controlled by flexure. The possibility of having a shear or joint type of failure should be checked employing other methods described in Section 3.1. The proposed method is limited to single strut models only. Further work is needed for the strut models where more than one strut element is used to model the masonry infill with gaps or openings.

Finally, the proposed method was applied to a set of RC case study frame structures with different infill typologies. Comparison with the response obtained with detailed numerical models showed that the proposed method efficiently captures the salient features of infilled frames with non-ductile failure mechanisms. In particular, the evolution of the displaced shape across the building height and the correct identification of critical storey locations were observed for many different case study structures. The incorporation of the strut flexibility, which was previously not considered in the literature, was shown to have a notable influence, and its consideration yielded accurate results. Comparing the performance of the proposed method with other similar approaches available in the literature highlighted its benefits and advantages, not just in terms of the final results but also how the further consideration via a pilotis potential index, infill demand index and consideration of the unloading stiffness may be used to improve existing approaches.

Acknowledgements

The work presented in this paper has been developed within the framework of the projects "Dipartimenti di Eccellenza", funded by the Italian Ministry of Education, University and Research at IUSS Pavia and "ReLUIS 2019-2021," funded by the Italian Department of Civil Protection.

References

1. Freeman SA. Prediction of response of concrete buildings to severe earthquake motion. ACI J. 1978;55(Special Publication):589–606.
2. Fajfar P. A nonlinear analysis method for performance-based seismic design. Earthq Spectra. 2000;16(3):573–92.
3. FEMA. FEMA 356: Prestandard and commentary for the seismic rehabilitation of buildings. 2000.
4. ATC. ATC-40: Seismic evaluation and retrofit of concrete buildings. ATC. 1996.
5. CEN. Eurocode 8: Design of structures for earthquake resistance - Part 1: General rules, seismic actions and rules for buildings Eurocode. Brussels, Belgium: European Committee for Standardization; 2004 p. 229.
6. Vamvatsikos D, Cornell CA. Direct estimation of the seismic demand and capacity of oscillators with multi-linear static pushovers through IDA. Earthq Eng Struct Dyn. 2006;35(9):1097–117.
7. Bellah Nafeh AM, O'Reilly GJ, Monteiro R. Simplified seismic assessment of infilled RC frame structures. Bull Earthq Eng. 2020;Accepted.

8. Cornell CA, Krawinkler H. Progress and challenges in seismic performance assessment. PEER Cent News. 2000;3(2):1–2.
9. McKenna F, Scott MH, Fenves GL. Nonlinear finite-element analysis software architecture using object composition. J Comput Civ Eng. 2010;24(1):95–107.
10. Seismosoft. SeismoStruct 2018 – A computer program for static and dynamic nonlinear analysis of framed structures. Pavia, Italy; 2018. p. 505.
11. Carr AJ. RUAUMOKO - User manual, theory, and appendices. 2007.
12. CSI. SAP2000 Integrated software for structural analysis and design. Computers and Structures Inc.; 2019.
13. Sullivan TJ, Saborio Romano D, O'Reilly GJ, Welch DP, Landi L. Simplified pushover analysis of moment resisting frame structures. J Earthq Eng. 2018;00(00):1–28.
14. Priestley MJN, Calvi GM. Towards a capacity-design assessment procedure for reinforced-concrete frames. Earthq Spectra. 1991;7(3):413–37.
15. Priestley MJN. Displacement-based seismic assessment of reinforced concrete buildings. J Earthq Eng. 1997;1(1):157–92.
16. Priestley MJN, Calvi GM, Kowalsky MJ. Displacement-based seismic design of structures. 1st Ed. Vol. 24. Pavia, Italy: IUSS Press; 2007. 721 p.
17. Shibata A, Sözen MA. Substitute-structure method for earthquake-resistant design or reinforced concrete frames. Engineering Studies. Urbana-Champaign; 1987.
18. Fenerci A, Binici B, Ezzatfar P, Canbay E, Ozcebe G. The effect of infill walls on the seismic behavior of boundary columns in RC frames. Earthq Struct. 2016;10(3):539–62.
19. Sassun K, Sullivan TJ, Morandi P, Cardone D. Characterising the in-plane seismic performance of infill masonry. Bull New Zeal Soc Earthq Eng. 2016;49(1):98–115.
20. Furtado A, Rodrigues H, Arêde A, Varum H. Experimental Characterization of the In-plane and Out-of-Plane Behaviour of Infill Masonry Walls. In: Procedia Engineering. Elsevier Ltd; 2015. p. 862–9.
21. Shing PB, Mehrabi AB. Behaviour and analysis of masonry-infilled frames. Prog Struct Eng Mater. 2002 Jul 1;4(3):320–31.
22. Calvi GM, Bolognini D. Seismic response of reinforced concrete frames infilled with weakly reinforced masonry panels. J Earthq Eng. 2001;5(2):153–85.
23. Chiou Y-J, Tzeng J-C, Liou Y-W. Experimental and Analytical Study of Masonry Infilled Frames. J Struct Eng. 1999 Oct 1;125(10):1109–17.
24. Crisafulli FJ. Seismic behaviour of reinforced concrete structures with masonry infills. University of Canterbury; 1997.
25. O'Reilly GJ, Sullivan TJ. Probabilistic seismic assessment and retrofit considerations for Italian RC frame buildings. Bull Earthq Eng. 2018 Mar 1;16(3):1447–85.
26. Perrone D, Leone M, Aiello MA. Evaluation of the infill influence on the elastic period of existing RC frames. Eng Struct. 2016 Sep 15;123:419–33.
27. Hak S, Morandi P, Magenes G, Sullivan TJ. Damage control for clay masonry infills in the design of RC frame structures. J Earthq Eng. 2012;16(SUPPL. 1):1–35.
28. Crisafulli FJ, Carr AJ, Park R. Analytical modelling of infilled frame structures - A general review. Bull New Zeal Soc Earthq Eng. 2000;33(1):30–47.
29. Thiruvengadam V. On the natural frequencies of infilled frames. Earthq Eng Struct Dyn. 1985 May 1;13(3):401–19.
30. Landi L, Tardini A, Diotallevi PP. A Procedure for the displacement-based seismic assessment of infilled RC frames. J Earthq Eng. 2016;20(7):1077–103.
31. Saborío Romano D. Performance based and simplified displacement-based assessments of an infilled RC frame building in L'Aquila, Italy. Istituto Universitario di Studi Superiori di Pavia; 2016.
32. Cardone D, Flora A. Multiple inelastic mechanisms analysis (MIMA): A simplified method for the estimation of the seismic response of RC frame buildings. Eng Struct. 2017;145:368–80.
33. Gentile R, Pampanin S, Raffaele D, Uva G. Non-linear analysis of RC masonry-infilled frames using the SLaMA method: part 1—mechanical interpretation of the infill/frame interaction and formulation of the procedure. Bull Earthq Eng. 2019;17(6):3283–304.
34. Priestley MJN, Ravindra V, Xiao Y. Seismic shear strength of reinforced concrete columns. J Struct Eng. 1994;120(8):2310–29.
35. Tasligedik AS, Akguzel U, Kam WY, Pampanin S. Strength Hierarchy at Reinforced Concrete Beam-Column Joints and Global Capacity. J Earthq Eng. 2018 Mar 16;22(3):454–87.
36. De Risi MT, Verderame GM. Experimental assessment and numerical modelling of exterior non-conforming beam-column joints with plain bars. Eng Struct. 2017 Nov 1;150:115–34.
37. Calvi G, Magenes G, Pampanin S. Relevance of beam-column joint damage and collapse in rc frame assessment. J Earthq Eng. 2002;6:75–100.

38. O'Reilly GJ, Sullivan TJ. Modeling techniques for the seismic assessment of the existing italian RC frame structures. J Earthq Eng. 2019;23(8):1262–96.
39. Mohamed H, Romão X. Analysis of the performance of strut models to simulate the seismic behaviour of masonry infills in partially infilled RC frames. Eng Struct. 2020 Nov 1;222:111124.
40. Di Trapani F, Shing PB, Cavaleri L. Macroelement Model for In-Plane and Out-of-Plane Responses of Masonry Infills in Frame Structures. J Struct Eng. 2018;144(2):04017198.
41. Ricci P, Di Domenico M, Verderame GM. Empirical-based out-of-plane URM infill wall model accounting for the interaction with in-plane demand. Earthq Eng Struct Dyn. 2018 Mar 1;47(3):802–27.
42. Bertoldi SH, Decanini LD, Gavarini C. Telaitamponatisoggetti ad azioni sismiche, un modelosemplificato: confronto sperimentale e numerico. In: Borri A, Perducci A, editors. Atti del 6 Convegno Nazionale L'ingegneria sismica in Italia. Perugia, Italy: Press Center of the University of Perugia; 1993. p. 815–24.
43. Decanini L, Mollaioli F, Mura A, Saragoni R. Seismic performance of masonry infilled R/C frames. In: 13th World Conference on Earthquake Engineering. Vancouver, B.C., Canada; 2004.
44. Panagiotakos TB, Fardis MN. Seismic response of infilled RC frames structures. In: Eleventh World Conference on Earthquake Engineering. Acapulco, Mexico: Elsevier Science Ltd; 1996.
45. Mucedero G, Perrone D, Brunesi E, Monteiro R. Numerical Modelling and Validation of the Response of Masonry Infilled RC Frames Using Experimental Testing Results. Build 2020, Vol 10, Page 182 [Internet]. 2020 Oct 13;10(10):182. Available from: https://www.mdpi.com/2075-5309/10/10/182/htm
46. Mohammad Noh N, Liberatore L, Mollaioli F, Tesfamariam S. Modelling of masonry infilled RC frames subjected to cyclic loads: State of the art review and modelling with OpenSees. Eng Struct. 2017 Nov 1;150:599–621.
47. Stafford Smith B, Carter C. A method of analysis for infilled frames. Proc Inst Civ Eng. 1969 Sep 17;44(1):31–48.
48. Asteris PG, Cotsovos DM, Chrysostomou CZ, Mohebkhah A, Al-Chaar GK. Mathematical micromodeling of infilled frames: State of the art. Eng Struct [Internet]. 2013;56:1905–21. Available from: http://dx.doi.org/10.1016/j.engstruct.2013.08.010
49. Antoniou S, Pinho R. Development and verification of a displacement-based adaptive pushover procedure. J Earthq Eng. 2004;8(5):643–61.
50. Stafford Smith B. Methods for predicting the lateral stiffness and strength of multi-storey infilled frames. Build Sci. 1967 Jan 1;2(3):247–57.
51. Crisafulli FJ, Carr AJ. Proposed macro-model for the analysis of infilled frame structures. Bull New Zeal Soc Earthq Eng. 2007;40(2):69–77.
52. Seismic Evaluation and Retrofit of Existing Buildings [Internet]. ASCE/SEI 4. Seismic Evaluation and Retrofit of Existing Buildings. American Society of Civil Engineers; 2017. Available from: https://ascelibrary.org/doi/10.1061/9780784414859
53. Bose S, Martin J, Stavridis A. Simulation Framework for Infilled RC Frames Subjected to Seismic Loads: https://doi.org/101193/042218EQS100M [Internet]. 2019 Nov 28;35(4):1739–62. Available from: https://journals.sagepub.com/doi/10.1193/042218EQS100M
54. Collins MP, Mitchell D. Prestressed concrete structures. Toronto, Ontario: Response Publications; 1997.
55. Akan OD. Displaced shapes of infilled RC frames for displacement-based design and assessment. Istituto Universitario di Studi Superiori di Pavia; 2019.
56. O'Reilly GJ, Sullivan TJ. Fragility functions for eccentrically braced steel frame structures. Earthq Struct. 2016;10(2):367–88.
57. Sullivan TJ, Calvi GM. Considerations for the seismic assessment of buildings using the direct displacement-based assessment approach. In: Associazione nazionale di ingegneria sismica in Italia (ANIDIS). Bari, Italy; 2011.
58. Hall JF. On the descending branch of the pushover curve for multistory buildings. Earthq Eng Struct Dyn. 2018;47(3):772–83.
59. Galli M. Evaluation of the seismic response of existing RC frame buildings with masonry infills. Istituto Universitario di Studi Superiori; 2006.
60. O'Reilly GJ, Kohrangi M, Bazzurro P, Monteiro R. Intensity measures for the collapse assessment of infilled RC frames. In: 16th European Conference on Earthquake Engineering. Thessaloniki, Greece; 2018.
61. Scott MH, Fenves GL. Plastic Hinge Integration Methods for Force-Based Beam–Column Elements. J Struct Eng. 2006 Feb 1;132(2):244–52.
62. ACI Committee 318. ACI CODE-318-19: Building Code Requirements for Structural Concrete and Commentary [Internet]. 2019. p. 624. Available from: https://www.concrete.org/store/productdetail.aspx?ItemID=318U19&Language=English

A. Appendix: Example application of the proposed procedure to a three-storey three-bay strong infilled RC frame with a column-sway mechanism

The proposed simplified procedure (Figure 4.1) is here applied in detail to the three-storey three-bay strong infilled RC frame structure shown in Figure 5.1. The procedure is fully demonstrated by evaluating the first point on the pushover curve of the structure, which is displayed in Figure 5.2. The calculations for the rest of the points are available in the spreadsheet made available cited in Section 5.

The flexural strength points (at joint centrelines) on the backbone curve of each structural element are shown in Figure A.1.a. It is assumed that beams and columns have enough shear strength to allow the development of plastic hinges. The flexural strengths of columns are based on gravity-induced axial loads and computed via moment-curvature analysis. The intermediate steps to calculate the storey shear contribution of the frame members are omitted for brevity. Interested readers should refer to the study by Sullivan et al. (13) for more detail. The equilibrium of flexural forces around each joint is shown in Figure A.1.b. The frame resistance is computed by summing over the flexural capacities of the column sections at each storey and scaling by the storey height. Equilibrium is obtained for the rest of the points to obtain the storey frame backbone.

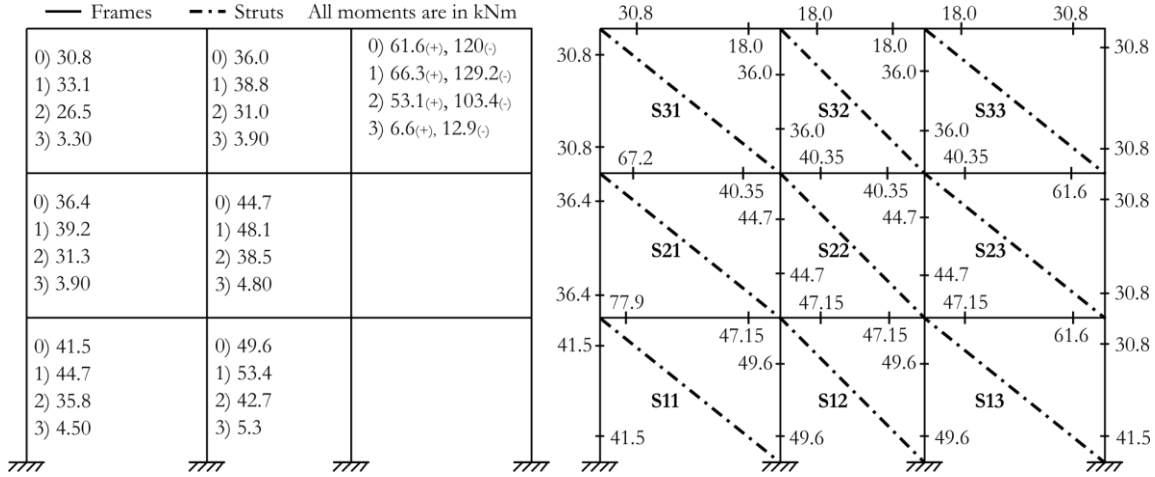

Figure A.1. a) Column and beam moment capacities of the frame members. Beam moments (+, -) are shown at the top right corner. All beam sections are the same and the columns are symmetric. Points 0-3 refer to the subsequent points in the backbone of each section. b) After joint equilibrium is achieved for the initial limit state

The frame storey shear, stiffness and drift values, computed following the methodology described by Sullivan et al. (13), are presented in Table A.1.

Table A.1. First three points of the storey frame backbone ψ_i computed through simplified analysis

Storey	Frame Damage State 0			Frame Damage State 1			Frame Damage State 2		
	F (kN)	K (kN/m)	θ (rad)	F (kN)	K (kN/m)	θ (rad)	F (kN)	K (kN/m)	θ (rad)
3	89	3093	0.0096	96	182	0.0220	77	-170	0.0597
2	104	3793	0.0092	112	192	0.0231	90	-281	0.0498
1	129	5774	0.0081	138	220	0.0244	111	-443	0.0472

In parallel, the infill contribution is computed by evaluating the axial strut strength and strain values (ε) (Table A.2) given by the chosen backbone model – Sassun et al. (19) in this case. Then, for each strut, the tangent stiffnesses in the global horizontal direction are computed. An example for the second storey is shown below.

Table A.2. The axial strut backbone for S21, the strut at the second storey first bay

Strut Damage State	0	1	2	3
f_{21} (kN)	256	320	32	32
k_{21} (kN/m)	59078	8440	-12331	0
ε_{21}	0.0008	0.0022	0.0089	0.02

For the initial limit, the contribution of the strut S21 from Figure A.1 to the global storey horizontal stiffness of the infilled frame is computed with Eqs. (3.8) and (3.9). The strut angle is denoted by λ, and it is given by the clear storey height divided by the clear bay length, shown in Figure 3.3. The ACI 318 (62) formula is used for the concrete modulus.

$$cos^2\lambda_{21} = (0.86)^2 = 0.74 \; where \; \lambda_{21} = \tan^{-1}\left(\frac{h_w}{l_w}\right) = \tan^{-1}\left(\frac{2.5\; m}{4.25\; m}\right) = 0.53\; rad$$

The contribution of infills to the lateral storey resistance at the second storey is computed as:

$$F^1_{infill,2} = f^1_{strut,(21)}cos\lambda_{21} + f^1_{strut,(22)}cos\lambda_{22} + f^1_{strut,(23)}cos\lambda_{23} = 2(256)(0.86) + (158)(0.57) = 531\; kN$$

The unit horizontal displacement of the strut at the second storey first bay due to a unit lateral force is:

$$\delta^1_{21} = \frac{1}{(cos^2\lambda_{21})\left(k^0_{strut,(21)}\right)} + \frac{tan^2\lambda_{21}}{k^0_{column,(21)}} + \frac{tan^2\lambda_{11}}{k^0_{column,(11)}} + \frac{tan^2\lambda_{12}}{k^0_{column,(12)}}$$

$$= \frac{1}{(0.74)(59078)} + \frac{(0.59)^2}{433496} + \frac{(0.59)^2}{472904} + \frac{(0.59)^2}{472904} = 2.5 \times 10^{-5} m$$

The axial stiffness contribution of the second-storey infills to the storey stiffness is:

$$K^0_{axial,2} = \frac{1}{\delta^1_{21}} + \frac{1}{\delta^1_{22}} + \frac{1}{\delta^1_{23}} = \frac{1}{(2.5 \times 10^{-5})} + \frac{1}{(6.88 \times 10^{-5})} + \frac{1}{(2.5 \times 10^{-5})} = 94394\; kN/m$$

The storey infill backbone is established by evaluating the infill resistance, tangent horizontal stiffness and the drift values, shown in Table A.3.

Table A.3. First three points of the storey infill backbone β_i computed through simplified analysis

Storey	Infill Damage State 0			Infill Damage State 1			Infill Damage State 2		
	F (kN)	K (kN/m)	θ (rad)	F (kN)	K (kN/m)	θ (rad)	F (kN)	K (kN/m)	θ (rad)
3	524	85649	0.0020	655	14270	0.0051	65	-19744	0.0150
2	531	**94394**	0.0019	664	14856	0.0049	66	-20418	0.0146
1	531	104818	0.0018	664	15500	0.0050	66	-21972	0.0149

Finally, Table A.1 and Table A.3 are combined, to obtain Table A.4, based on the parallel springs assumption presented in Figure 3.2. First, the damage states identified in both frame and infill steps are sorted in ascending order based on the drift values. Then, the stiffness pair associated with each system damage state is summed. An example for the system damage state 0 and 1 of the second storey is shown below:

$$K^0_{system,2} = K^0_{flexural,2} + K^0_{axial,2} = 3793 + 94394 = 98187\ \text{kN/m}$$

$$K^1_{system,2} = K^0_{flexural,2} + K^1_{axial,2} = 3793 + 14856 = 18649\ \text{kN/m}$$

The limit storey shear resistance associated with the system damage state is computed using the limit drift and the state stiffness, as shown here for the damage state 1 of the second storey:

$$F^2_{system,2} = F^1_{sysytem,2} + K^1_{system,2}.\left(\theta^2_{system,2} - \theta^1_{system,2}\right).h_{storey,2}$$

$$= 553 + 18649 \cdot (0.0049 - 0.0019) \cdot (3) = 719\; kN$$

Table A.4. First three damage states of the storey system backbone ζ_i computed through simplified analysis

System Damage S.	Storey 1				Storey 2				Storey 3			
	DS	$F_{sys.}$	$\theta_{sys.}$	$K_{sys.}$	DS	$F_{sys.}$	$\theta_{sys.}$	$K_{sys.}$	DS	$F_{sys.}$	$\theta_{sys.}$	$K_{sys.}$
0	Inf.-0	561	0.0018	110592	Inf.-0	553	0.0019	**98187**	Inf.-0	543	0.0020	88742
1	Inf.-1	743	0.0050	21274	Inf.-1	**719**	0.0049	**18649**	Inf.-1	702	0.0051	17363
2	Fr.-0	603	0.0081	-16198	Fr.-0	504	0.0092	-16625	Fr.-0	477	0.0096	-16651

Table A.4, completes the modelling part. Before starting with the analysis part, the sway potential index, S_p and pilotis potential index, P_p, are computed as in Table A.5. As an example, P_p for joint level 1 is computed as:

$$P^{above}_{p,1} = \frac{\left(\sum M_{inifll,i}\right)h_{storey,(i+1)}(N-i)}{\sum M^{bottom}_{column,(i+1)}\left(\sum_{a=i}^{N}(\sum_{b=a}^{N} h_{s,b})\right)} = \frac{(531 \times 2.75) \cdot (3.0) \cdot (2)}{(30.8 + 2 \times 44.7 + 36.4) \cdot (17.75)} = 3.15$$

$$P_{p,1}^{below} = \frac{\left(\sum M_{inifll,(i+1)}\right) h_{storey,i}(N+1-i)}{\sum M_{column,i}^{top}\left(\sum_{a=i}^{N}(\sum_{b=a}^{N} h_{s,b})\right)} = \frac{(531 \times 3.0)\cdot(2.75)\cdot(3)}{(30.8+2\times 49.6+41.5)\cdot(17.75)} = 4.32$$

The expected frame inelastic mechanism can be checked using Table A.5. Note that, during the frame computations above, the column-sway drift equation proposed by Sullivan et al. (13) is employed while computing the drift limits of the frame members. Since Table A.5 does indicate a column sway mechanism at each floor, the computed frame capacities do not need revision. Furthermore, in case of a beam-sway frame, the frame drift limits would be updated at this step using the proper equation (i.e., column-sway equation). In the example above the contribution of infill moments at other storeys is not included since the ratio is already greater than unity.

Table A.5. Sway potential index, S_p and Pilotis potential index, P_p

Level	Sp	$P_{p,1}^{above}$	$P_{p,1}^{below}$	Sway Mechanism	$\Sigma M_{col.}^{bottom}$ (kNm)	$\Sigma M_{col.}^{top}$ (kNm)	ΣM_{infill} (kNm)	h_{stry} (m)	Σh_{stry} (m)	OTM (kNm)
3	4.08	n.a.	n.a	Column	n.a.	134	1571	3	3	3
2	1.84	3.98	6.69	Column	134	157	1594	3	6	9
1	1.58	**3.15**	**4.32**	Column	157	172	1461	2.75	8.75	17.75

After verifying that the expected mechanism, column sway, is in agreement with the frame capacity calculation method at each floor, the analysis of the infilled frame is started. Evaluating the displacement and shear profile for a target base shear $V_b^{target} = F_{system,1}^{1} = 560\ kN$:

- Step 1. Estimate a guess displacement profile; either linear ($\Delta_i^t = \theta_{guess} H_{storey}$) or the committed profile at the end of the previous step ($\Delta_i^t = \Delta_i^{t-1}$), if available. Take initial $\theta_{guess} = 0.001\ rad$;
- Step 2. Compute the storey shear demand profile V_i^t for Δ_i^t using Eqs. (4.3) and (4.4);

Table A.6. Calculations of steps 1-2 for the initial point on the pushover curve

Storey	Δ_i^t (m)	m_i	F_i^t (kN)	V_i^t (kN)	$F_{fr,i}^t$ (kN)	$F_{inf,i}^t$ (kN)	S_{Di}	I_{Di}	$V_{true,i}^t$ (kN)	ΔV
3	0.0088	38	275	275	9	250	0.10	0.48	260	15.3
2	0.0058	40	193	468	11	280	0.11	0.53	291	176.2
1	0.0028	40	92	560	16	297	0.12	0.56	313	247.0

- Step 3. Obtain a new displacement profile Δ_i^{t+1} using Eqs. (4.5) and (4.6);
- Step 4. Compute the new storey shear demand profile V_i^{t+1}. Compute the sway (S_{Di}) and infill (I_{Di}) demand indices for each storey and revise the base shear;

Table A.7. Calculations of steps 3-6 for the initial point (iterations 1-2)

Storey	V_i^{t+1} (kN)	$K_{sys,i}^k$ (kN/m)	δ_i^{t+1} (m)	Δ_i^{t+1} (m)	ΔV	V_i^{t+1} (kN)	δ_i^{t+1} (m)	Δ_i^{t+1} (m)	ΔV
3	275	86553	0.0032	0.0129	-21.7	250	0.0029	0.0125	-2.9
2	468	97140	0.0048	0.0097	-10.8	455	0.0047	0.0096	-1.8
1	560	113758	0.0049	0.0049	0.0	560	0.0049	0.0049	0.0

- Step 5. Evaluate the storey unbalanced load using Eqs. (4.7) and (4.8). Repeat the calculation from step 3 until the unbalanced load is zero at every floor and S_{Di} or I_{Di} at a level reach unity. Consider a new estimate of base shear equal to the target base shear (before step 1) divided by the maximum sway or infill demand index;
- Step 6. When an infill or frame member reach capacity at a floor, update the member's resistance, drift and stiffness. Finally, mark the base shear vs roof displacement point on the pushover curve and repeat from step 1 for a new target base shear estimate.

Table A.8. Calculations of steps 3-6 for the initial point (iteration 3) and values after convergence

Storey	V_i^{t+1} (kN)	δ_i^{t+1} (m)	Δ_i^{t+1} (m)	V_i^{t+1} (kN)	$F_{fr,i}^{t+1}$ (kN)	$F_{inf,i}^{t+1}$ (kN)	S_{Di}	I_{Di}	ΔV
3	250	0.0029	**0.0125**	250	9	241	0.10	0.46	-0.4
2	455	0.0047	0.0096	455	18	437	0.17	0.82	-0.3
1	560	0.0049	0.0049	560	28	531	0.22	**1.00**	0.0

In Table A.8, after convergence, the initial point on the pushover curve is identified as follows:

$$For\ \Delta_{\boldsymbol{roof}}^{\boldsymbol{t}} = 0.0125\ m \rightarrow V_{SDOF} = M_{OTM}/H_{eff.} = (250 \times 3 + 455 \times 3 + 560 \times 2.75)/6.53 = 560\ kN$$

Since the I_{Di} at the first level has reached unity after convergence is achieved, the damage state of the level is updated. From now on, the updated mechanical properties of the first floor will be used in the iterations. For the next point on the pushover curve, the previous procedure is repeated with the updated mechanical parameters of the first floor.